Check for updates

JGR Space Physics

RESEARCH ARTICLE
10.1029/2026JA036129

Induction Signals From Europa's Subsurface Ocean: Contributions of Time Variations in the Plasma Interaction

Lucas Liuzzo[1], **Sven Simon**[2,3], **C. Michael Haynes**[2], **and Andrew R. Poppe**[1]

[1]Space Sciences Laboratory, University of California, Berkeley, CA, USA, [2]School of Earth and Atmospheric Sciences, Georgia Institute of Technology, Atlanta, GA, USA, [3]School of Physics, Georgia Institute of Technology, Atlanta, GA, USA

Key Points:

- We combine an analytic and computational approach to quantify Europa's inductive response to its time-varying plasma environment
- Induction by time-varying plasma currents generates signals comparable to those associated with uncertainties in properties of an ocean
- Perturbations associated with this response are discernible at Europa Clipper flyby altitudes and must be quantified during each encounter

Correspondence to:
L. Liuzzo,
liuzzo@berkeley.edu

Citation:
Liuzzo, L., Simon, S., Haynes, C. M., & Poppe, A. R. (2026). Induction signals from Europa's subsurface ocean: Contributions of time variations in the plasma interaction. *Journal of Geophysical Research: Space Physics*, *131*, e2026JA036129. https://doi.org/10.1029/2026JA036129

Received 24 AUG 2026
Accepted 19 OCT 2026

Author Contributions:
Conceptualization: Lucas Liuzzo, Sven Simon, C. Michael Haynes
Data curation: Lucas Liuzzo
Formal analysis: Lucas Liuzzo, Sven Simon, C. Michael Haynes
Funding acquisition: Lucas Liuzzo, Sven Simon
Investigation: Lucas Liuzzo, Sven Simon
Methodology: Lucas Liuzzo, Sven Simon, C. Michael Haynes, Andrew R. Poppe
Project administration: Lucas Liuzzo, Sven Simon
Resources: Lucas Liuzzo

© 2026 The Author(s). Journal of Geophysical Research: Space Physics published by Wiley Periodicals LLC on behalf of American Geophysical Union. This is an open access article under the terms of the Creative Commons Attribution-NonCommercial License, which permits use, distribution and reproduction in any medium, provided the original work is properly cited and is not used for commercial purposes. All other rights reserved, including rights for text and data mining and training of artificial intelligence technologies or similar technologies.

Abstract The magnetic perturbations generated by Europa's plasma interaction undergo oscillatory variations since Jupiter's magnetospheric current sheet periodically sweeps across the moon. We determine the inductive response of Europa's subsurface ocean to this excitation signal and compare it to the field induced by the time-varying yet locally uniform Jovian background field. We apply a hybrid model to calculate the three-dimensional structure of Europa's plasma and electromagnetic environment at equidistant points in time across a Jovian synodic rotation. We isolate the time-varying component of this interaction to calculate the resulting induced Gauss coefficients, then evaluate the feedback of this field on the plasma perturbations. We find that induction by time-varying plasma currents generates largely dipolar contributions to Europa's magnetic environment that cause discernible modifications to the moon's plasma interaction. The effect of these induced fields is strongest near the center of Jupiter's magnetospheric current sheet. In this scenario, the inductive response to the uniform magnetospheric background field is minimized while the magnetic signatures from the deflection of the upstream flow maximize. Finally, we illustrate that the fields induced by time-varying plasma currents can nearly equal the fields induced by the time-varying magnetospheric fields within the current sheet, even at flyby altitudes. For all distances of the moon with respect to the sheet, these plasma-induced fields are comparable to the induction signal from, for example, fluid convection within the ocean or deviations of the ocean's shape from a perfect sphere. Hence, this effect must be included when characterizing Europa's interior through magnetometer measurements.

1. Introduction

Europa (radius R_E = 1561 km) orbits deep within Jupiter's magnetosphere at a distance of 9.38R_J (radius of Jupiter: R_J = 71492 km). The 9.6° tilt of Jupiter's magnetic moment against its rotation axis drives periodic changes to the local magnetospheric field near the moon. Hence, the magnetic environment near Europa is highly variable, oscillating with a time scale dominated by the planetary synodic rotation period of 11.23 hr (e.g., Seufert et al., 2011; Vance et al., 2021). This time variability induces currents within Europa's conducting subsurface ocean, generating measurable distortions of the magnetospheric field outside of the moon (e.g., Khurana et al., 1998; Kivelson et al., 1997, 1999, 2000). The magnitude and orientation of the induced field change periodically as the Jovian magnetic current sheet continuously sweeps over the moon at the synodic period.

When treating the local ambient Jovian field as spatially uniform and assuming the subsurface ocean layer to be spherically symmetric, Europa's induced field can be represented by a time-varying dipole moment centered at Europa (Saur et al., 2010; Zimmer et al., 2000). Using magnetic field observations from the Galileo flybys, early studies confirmed the existence of the moon's ocean by treating it as a perfect conductor (e.g., Kivelson et al., 2000). Subsequently, Zimmer et al. (2000) extracted the magnitude and phase lag of the induced magnetic moment from magnetometer data acquired during the Galileo E4 and E14 encounters and found that the field induced at Europa is (at least) as strong as 70% of the field expected for a perfectly conducting sphere of the same radius as the moon. They concluded that the ocean must be located at a depth of 200–300 km beneath the surface with a conductivity of at least 60 mS/m.

The detectability of the magnetic field induced within Europa's subsurface ocean is severely complicated by the field perturbations from currents generated by the interaction with the Jovian magnetospheric plasma to which the moon is persistently exposed. Europa's orbital period is significantly larger than Jupiter's rotational period, so the moon is continuously overtaken by the (partially) corotating flow at a relative velocity of about 100 km/s (Bagenal & Dols, 2020; Bagenal et al., 2015; Kivelson et al., 2009). Hence, Europa's surface, ionosphere, and induced field

21699402, 2026, 11, Downloaded from https://agupubs.onlinelibrary.wiley.com/doi/10.1029/2026JA036129 by Georgia Institute Of Technolog, Wiley Online Library on [09/11/2026]. See the Terms and Conditions (https://onlinelibrary.wiley.com/terms-and-conditions) on Wiley Online Library for rules of use; OA articles are governed by the applicable Creative Commons License

Software: Lucas Liuzzo, Andrew R. Poppe
Validation: Lucas Liuzzo, Sven Simon, C. Michael Haynes, Andrew R. Poppe
Visualization: Lucas Liuzzo
Writing – original draft: Lucas Liuzzo, Sven Simon
Writing – review & editing: Lucas Liuzzo, Sven Simon, C. Michael Haynes, Andrew R. Poppe

represent obstacles to the impinging magnetospheric plasma flow. As such, the Jovian magnetospheric field lines pile-up near the moon's ramside hemisphere and form an extended draping pattern above its poles, connecting to a system of Alfvén wings at larger distances (Neubauer, 1980, 1998). This plasma interaction gives rise to additional perturbations of up to 100–200 nT in individual field components, deforming and partially obscuring any induction signal (e.g., Addison et al., 2024; Baskevitch et al., 2025; Harris et al., 2021; Jia et al., 2018; Rubin et al., 2015; Schilling et al., 2008). When Europa is located away from the center of Jupiter's magnetospheric plasma sheet, the density of the impinging flow is minimized and the currents generated by the moon's plasma interaction are weak (Bagenal & Delamere, 2011; Haynes et al., 2023; Roth et al., 2014). In this case, the presence (but not necessarily the strength or orientation) of the induced dipole moment may be discernible in magnetometer data from close flybys along certain trajectories (Schilling et al., 2007; Zimmer et al., 2000). By comparison, the elevated density of the incident magnetospheric plasma near the center of the Jovian plasma sheet results in strong currents generated by the plasma interaction that may completely obscure the induced field in certain regions (Addison et al., 2024; Arnold, Liuzzo, & Simon, 2020; Rubin et al., 2015).

In addition, the resulting plasma interaction and induction effects are coupled in a highly non-linear way. First, compared to a (hypothetical) scenario without induction, the induced field reduces the cross-sections of the Alfvén wing tubes, slightly displaces the wings against the center of the moon's disk (Arnold, Liuzzo, & Simon, 2020; Neubauer, 1999; Volwerk et al., 2007), and reduces the magnitude of the currents along their characteristics (Neubauer, 1999). Second, the time variability of the plasma currents themselves induces additional currents within Europa's interior: as Jupiter's magnetospheric plasma sheet sweeps over the moon at the synodic rotation period, the upstream density (Bagenal & Delamere, 2011; Bagenal et al., 2015; Kurth et al., 2001) and magnetic field (Khurana et al., 2009) change in time. This variability causes, for example, the strength of the magnetic pile-up at Europa's ramside as well as the magnitude and inclination of the currents within the Alfvén wings to oscillate at the synodic period.

Schilling et al. (2007) developed an MHD model that self-consistently couples Europa's plasma interaction to the induced field from its interior and applied this model to understand magnetometer data from several Galileo flybys. These authors determined that an ocean conductivity of at least ∼0.5 S/m is required to reproduce the field perturbations detected in magnetometer observations. This threshold is nearly 10 times higher than the value obtained from Zimmer et al. (2000) that used data from the same Galileo encounters. Hence, it is imperative to include the contribution of these plasma interaction effects when quantifying properties of the moon's subsurface using magnetometer data. Schilling et al. (2007) found that the dipolar and quadrupolar Gauss coefficients induced by the time variability of Europa's plasma interaction are on the order of 10–20 nT. However, these authors did not calculate the magnetic fields outside of Europa associated with this inductive response, nor isolate the influence of this field on the plasma perturbations beyond the moon's surface.

A major goal of NASA's Europa Clipper mission is to constrain properties of the moon's subsurface ocean using magnetic field data from individual flybys (Kivelson et al., 2023). Various studies have estimated the degree to which non-uniformities in the ocean layer would alter the inductive response near Europa. Differences in the assumed composition of the ocean layer or radial gradients in the conductivity of the ocean would be responsible for perturbations on the order of ∼40 nT at the surface (Vance et al., 2021), while motional induction (by thermal convection within the ocean) would generate perturbations of up to 20 nT on the surface (Šachl et al., 2024). Additional "pockets" of water located between the ocean and Europa's surface may be responsible for an additional modification of ∼10 nT at altitudes of ∼25 km (Winkenstern & Saur, 2023), while a slightly elliptical ocean would cause deviations on the order of 2 nT as visible on the surface (Styczinski et al., 2022; Styczinski & Harnett, 2021). The contribution of any induced fields from Europa's dilute ionosphere is expected to be orders of magnitude weaker than currents generated by these other processes (approximately 0.5%; see Hartkorn & Saur, 2017; Vance et al., 2021).

Hence, at the expected altitude of the Europa Clipper encounters, any magnetic signatures associated with, for example, a non-spherical ocean shape or a localized pocket of water may not exceed the typical noise floor of the Jovian magnetospheric fluctuations on the order of 3–5 nT (Styczinski et al., 2022; Winkenstern & Saur, 2023). Any such geophysical signatures therefore could not be unambiguously detected by the spacecraft's magnetometer. On the other hand, deviations of the induction signal from a perfectly conducting, uniform Europa driven by, for example, a radial gradient to the ocean's conductivity or fluid convection within the ocean may exceed the

21699402, 2026, 11, Downloaded from https://agupubs.onlinelibrary.wiley.com/doi/10.1029/2026JA036129 by Georgia Institute Of Technolog, Wiley Online Library on [09/11/2026]. See the Terms and Conditions (https://onlinelibrary.wiley.com/terms-and-conditions) on Wiley Online Library for rules of use; OA articles are governed by the applicable Creative Commons License

background noise in the field and could potentially be identified at flyby altitudes. The observable induction signal may also contain discernible information on ocean composition (Vance et al., 2021).

Importantly, models of Europa's plasma interaction suggest that magnetometer data from close Clipper encounters (even at large distances to Jupiter's plasma sheet) may be "contaminated" by plasma effects to a significant degree (Addison et al., 2024; Arnold et al., 2019; Cervantes & Saur, 2022; Cervantes et al., 2025; Harris et al., 2021, 2022; Schilling et al., 2007). Due to the non-linear coupling between the plasma interaction and resulting inductive response (Neubauer, 1999; Schilling et al., 2007), the contribution of plasma currents cannot be subtracted from a magnetometer time series to retrieve a "pristine" induction signal. Thus, constraining the contribution of not only the plasma effects themselves, but also the inductive response associated with their time variability, is critical for any meaningful extraction of information on Europa's subsurface ocean from Clipper magnetometer data (Petricca et al., 2026). Furthermore it is imperative to identify spatial regions near Europa (and any corresponding segments of the Clipper trajectory) where the induced field generated by the time-varying plasma interaction is particularly strong.

Therefore, this study aims to quantify Europa's inductive response to the time variability of the moon's plasma interaction and identify locations near the surface that are strongly affected by these signatures. Such regions correspond to areas that may be challenging to use Europa Clipper magnetometer data to quantify properties of the subsurface ocean. This study is organized as follows: Section 2 introduces the analytical and numerical models that are applied to constrain Europa's plasma interaction and inductive response. Next, Section 3 contains results from this study in two iterations, first introducing a (hypothetical) scenario where the moon's inductive response does not contain contributions from the time-varying plasma interaction. These results are then compared against a (more realistic) scenario where the time-varying interaction induces currents within Europa and alters the local magnetic field environment. Finally, Section 4 summarizes our findings, placing emphasis on the observability of Europa's inductive response during the upcoming encounters of the Clipper mission.

2. Model Description

Our study employs the Cartesian EPhiO coordinate system (x, y, z) which is centered at Europa. The $(+x)$ axis of this system is aligned with the corotation direction while the $(+y)$ axis points toward Jupiter. The $(+z)$ axis completes the right-handed system and is oriented northward. We use symbols $\{\mathbf{e}_x, \mathbf{e}_y, \mathbf{e}_z\}$ to denote the unit basis vectors of the EPhiO system. Positions in this system are indicated by the vector $\mathbf{r} = (x, y, z)$. In addition, the calculation of Europa's inductive response is most straightforward in spherical polar coordinates (r, ϑ, ϕ), which we define through $x = r \sin\vartheta \cos\phi$, $y = r \sin\vartheta \sin\phi$, and $z = r \cos\vartheta$.

2.1. Induction by Time-Varying Plasma Currents: An Iterative Approach

While the inducing field at Europa contains a superposition of multiple excitation periods (e.g., Seufert et al., 2011), we proceed analogously to Schilling et al. (2007) and consider only ambient field variations at Jupiter's synodic rotation period of $T = 2\pi/\Omega \approx 11.23$ h (where Ω is the synodic frequency). This is the only excitation signal that generates an inductive response clearly exceeding 3% of the magnetospheric background field (Vance et al., 2021). Therefore, the induced field associated with the synodic signal is likely the only contribution that is not largely obstructed by the plasma interaction or random magnetospheric fluctuations (see, e.g., Winkenstern & Saur, 2023).

Our model includes two distinct contributions to the induction signal from Europa's interior. The first stems from the inductive response to the time-varying Jovian magnetospheric field $\mathbf{B}_0$ near the moon. On the length scales of Europa's plasma interaction region, this exciting field can be treated as spatially uniform (e.g., Addison et al., 2021; Rubin et al., 2015). In addition, the resulting induction signal can be approximated as constant in time when investigating its role in shaping Europa's plasma interaction: the incident magnetospheric flow requires only a few minutes to travel through the moon's local environment (e.g., Arnold, Liuzzo, & Simon, 2020). We analyze a "best-case" scenario where the induced field from Europa's interior is maximized; that is, the moon is treated as a perfectly conducting sphere of radius $1R_E$. This assumption does represent a suitable approximation to describe available observations in the moon's magnetic environment: numerous modeling studies of the plasma interaction have demonstrated that the magnitudes and extensions of the magnetic signatures seen during the Galileo and Juno flybys are compatible with such a description of the interior (e.g., Addison et al., 2021, 2024; Arnold

21699402, 2026, 11, Downloaded from https://agupubs.onlinelibrary.wiley.com/doi/10.1029/2026JA036129 by Georgia Institute Of Technolog, Wiley Online Library on [09/11/2026]. See the Terms and Conditions (https://onlinelibrary.wiley.com/terms-and-conditions) on Wiley Online Library for rules of use; OA articles are governed by the applicable Creative Commons License

et al., 2019; Harris et al., 2021, 2022; Rubin et al., 2015). Besides, in their recent analysis of magnetometer data from the Juno flyby, Cervantes et al. (2025) applied a multi-layer model of Europa's interior to calculate the inductive response to time variations of $\mathbf{B}_0$. These authors showed that the resulting amplitude of the induction signal is 96% that of the response expected for a perfectly conducting sphere, thereby further corroborating our choice. For a spherically symmetric conductor, exposed to a spatially uniform excitation signal, the induced field from the synodic variation of $\mathbf{B}_0$ can be represented by a dipole moment $\mathbf{M}$, centered at Europa. An expression for $\mathbf{M}$ is given by, for example, Neubauer (1998), Liuzzo et al. (2016), or Addison et al. (2021), and Section 2.3 also provides additional discussion.

Using a static dipole moment $\mathbf{M}$ to describe the induced field above Europa's surface is based on the notion of the moon being exposed to a vacuum. In a subsequent step, this dipole moment is therefore included in a model representing Europa's perturbed environment to calculate the moon's interaction with the incident magnetospheric flow (e.g., Harris et al., 2021; Haynes et al., 2023). However, the magnetic signatures generated by this interaction are also inherently time-varying. As the Jovian magnetospheric plasma sheet sweeps across the moon with period T, changes to Europa's local environment cause the Alfvénic Mach number M_A of the incident flow—and hence, the orientations of the Alfvén wing characteristics—to change periodically on the same time scale (Neubauer, 1980, 1999). The strength of the magnetic pile-up at Europa's ramside oscillates with period T as well (e.g., Addison et al., 2023; Harris et al., 2021; Haynes et al., 2023). This time variability causes a second (much weaker) induction signal from the subsurface ocean that is superimposed on the dipole moment $\mathbf{M}$ from the periodic change of $\mathbf{B}_0$ (Schilling et al., 2007). In the following, we lay out our strategy for determining this additional contribution to the induced field as well as its influence on the plasma flow deflection.

To emulate the magnetic signatures of the plasma interaction, we use the AIKEF hybrid model (Müller et al., 2011). This approach has an extensive history of applications to Europa (Addison et al., 2021, 2022, 2023, 2024; Arnold, Liuzzo, & Simon, 2020; Arnold, Simon, & Liuzzo, 2020; Arnold et al., 2019; Haynes et al., 2023, 2025). For the numerical details of AIKEF, the reader is therefore referred to any of our preceding publications, while specifics on the input parameters used in this study are discussed in Section 2.2. Our setup is based on the iterative approach of Schilling et al. (2007): we first apply AIKEF to determine the excitation signal from the time variability of the plasma currents near Europa. The analytical formalism introduced in Section 2.3 is then used to calculate the associated inductive response. To isolate any time variations in the plasma interaction (over the course of a synodic period T), we carry out an initial series of eight AIKEF runs. The initial conditions for these setups are chosen such that each represents a distinct distance between the moon and the center of Jupiter's magnetospheric plasma sheet, equally spaced (in time) across a synodic rotation T. The upstream conditions in each AIKEF run are kept constant in time and the effect of time variabilities is subsequently assessed by combining output from several model scenarios. Model runs are carried out for $\Omega t = 0°, 45°, 90°, \ldots, 315°$, where $t = 0$ denotes the point in time when Europa is far below the plasma sheet. This initial series of AIKEF runs considers only the internal magnetic moment induced by the time-varying, yet uniform magnetospheric background field $\mathbf{B}_0(t)$. For each of the eight setups, the ambient field vector $\mathbf{B}_0(t)$ is obtained from the empirical models of Connerney et al. (2020, 2022), which are based on observations from the Juno mission.

The output of these eight AIKEF runs is then used to determine the inducing field at Europa's surface $r = R_E$, caused by the time variability of the plasma currents. For this purpose, we decompose the magnetic field output $\mathbf{B}(x, y, z)$ from each of the eight runs according to

$$\mathbf{B} = \mathbf{B}_0 + \mathbf{B}_p + \mathbf{B}_{\text{ind}}(\mathbf{B}_0) + \mathbf{B}_{\text{ind}}(\mathbf{B}_p), \tag{1}$$

where $\mathbf{B}_p$ represents the spatially non-uniform perturbations caused by the (steady-state) plasma currents. The contributions $\mathbf{B}_{\text{ind}}(\mathbf{B}_0)$ and $\mathbf{B}_{\text{ind}}(\mathbf{B}_p)$ refer to the fields induced by the time variabilities of the uniform background field $\mathbf{B}_0$ and the plasma interaction fields $\mathbf{B}_p$, respectively. We note that in this initial series of eight runs, the term $\mathbf{B}_{\text{ind}}(\mathbf{B}_p)$ is assumed to be zero. However, as will be discussed below, this contribution will assume non-zero values in subsequent iteration cycles with AIKEF.

By taking the AIKEF output at each of the eight Ωt values and subtracting both the magnetospheric background field and its associated induced (dipole) field, we isolate the fields from plasma currents and their contribution to the induced field:

$$\widetilde{\mathbf{B}} = \mathbf{B} - \mathbf{B}_0 - \mathbf{B}_{\text{ind}}(\mathbf{B}_0) = \mathbf{B}_p + \mathbf{B}_{\text{ind}}(\mathbf{B}_p). \tag{2}$$

After averaging the field $\widetilde{\mathbf{B}}$ over a full synodic period T, we then determine the time-varying component $\widetilde{\mathbf{B}}_t$ of the perturbations generated by Europa's plasma interaction:

$$\widetilde{\mathbf{B}}_t = \underbrace{\mathbf{B}_p + \mathbf{B}_{\text{ind}}(\mathbf{B}_p)}_{(*)} - \underbrace{\langle \mathbf{B}_p + \mathbf{B}_{\text{ind}}(\mathbf{B}_p) \rangle}_{(**)}, \tag{3}$$

where the time average (denoted by the symbol $\langle \dots \rangle$) takes into account output from all eight AIKEF runs:

$$\langle \mathbf{B}_p + \mathbf{B}_{\text{ind}}(\mathbf{B}_p) \rangle = \frac{1}{T}\int_0^T \{\mathbf{B}_p + \mathbf{B}_{\text{ind}}(\mathbf{B}_p)\}\,\mathrm{d}t = \frac{1}{8}\sum_{j=1}^{8}\left\{\mathbf{B}_p^{(j)} + \mathbf{B}_{\text{ind}}^{(j)}(\mathbf{B}_p)\right\}. \tag{4}$$

The superscript (j) in the final expression of Equation 4 refers to the magnetic field output of AIKEF run $\#j \in \{1, 2, \dots, 8\}$. The second term $(**)$ in Equation 3 establishes a time-averaged "baseline" for the plasma interaction signatures that does not change over time (and hence, does not generate an induction signal), while the first term $(*)$ denotes the output from an individual AIKEF run. The quantity $\widetilde{\mathbf{B}}_t$ therefore describes the deviation of that field from the baseline.

By expanding these eight samples of $\widetilde{\mathbf{B}}_t$ into a discrete Fourier series, we then obtain the inducing field generated by the time variability of the plasma currents at any point in time during a synodic period T. Decomposition of the inducing field at Europa's surface into spherical harmonics then yields the field induced by time-varying plasma currents at any t during the synodic rotation (see Section 2.3).

Subsequently, a second set of AIKEF runs for the eight chosen distances to Jupiter's plasma sheet is carried out. However, in addition to the induced field $\mathbf{B}_{\text{ind}}(\mathbf{B}_0)$ from the time variation of $\mathbf{B}_0$, these runs also include the inductive response $\mathbf{B}_{\text{ind}}(\mathbf{B}_p)$ to the time-varying contribution of the plasma interaction. Analogous to our treatment of $\mathbf{B}_{\text{ind}}(\mathbf{B}_0)$, the induced field generated by the time-varying plasma currents is treated as constant during the transit time of the magnetospheric flow through Europa's interaction region (which defines the duration of an AIKEF run). By again using Equations 1–4, this second series of AIKEF runs produces refined results for $\widetilde{\mathbf{B}}_t$ and the associated induction signal. This iterative cycle needs to be repeated until convergence is achieved; that is, until the Gauss coefficients of $\mathbf{B}_{\text{ind}}(\mathbf{B}_p)$ from consecutive series of AIKEF runs differ by no more than 10% from each other. Similar to Schilling et al. (2007), we found that the second cycle of AIKEF runs (i.e., the first sequence that includes the field induced by time-varying plasma currents) is already sufficient to drive the iteration into convergence: the results for $\mathbf{B}_{\text{ind}}(\mathbf{B}_p)$ extracted from a third set of AIKEF runs differ only incrementally from those obtained in the second round.

2.2. Hybrid Model of Europa's Plasma Interaction

To represent the currents associated with Europa's plasma interaction, we apply the AIKEF hybrid model. For each of the eight distances to Jupiter's plasma sheet, we use a Cartesian domain with a spatial extent of $-9R_E \le x \le 21R_E$, $-10R_E \le y \le 10R_E$, and $-30R_E \le z \le 30R_E$. To adequately resolve, for example, Europa's atmospheric scale height, we apply a hierarchical grid resolution with two levels of refinement, resulting in a resolution of $\sim 0.02R_E$ for $|y, z| \le 3R_E$ and $-1.5 \le x \le 4.5$, a resolution of $\sim 0.04R_E$ for $|y, z| \le 4R_E$ and $-3R_E \le x \le 6R_E$, and a resolution of $\sim 0.09R_E$ elsewhere. The simulations use inflow conditions at the $-x$ boundary (at which the uniform properties of the ambient plasma is continuously injected), and outflow conditions elsewhere (at which the plasma leaves the domain). For high-resolution in velocity space, the simulations use ~ 100 macroparticles in every grid cell. Each scenario is stopped once the simulation reaches a quasi-stationary state, where the signatures associated with the interaction are no longer changing appreciably. All simulations are run to an identical point in time, until the incident plasma covers a distance that is ~ 1.5 larger than the AIKEF domain in the x-direction (corresponding to approximately 10 min of real time). This allows us to perform a one-to-one comparison of the output between different simulations.

21699402, 2026, 11, Downloaded from https://agupubs.onlinelibrary.wiley.com/doi/10.1029/2026JA036129 by Georgia Institute Of Technolog, Wiley Online Library on [09/11/2026]. See the Terms and Conditions (https://onlinelibrary.wiley.com/terms-and-conditions) on Wiley Online Library for rules of use; OA articles are governed by the applicable Creative Commons License

21699402, 2026, 11, Downloaded from https://agupubs.onlinelibrary.wiley.com/doi/10.1029/2026JA036129 by Georgia Institute Of Technolog, Wiley Online Library on [09/11/2026]. See the Terms and Conditions (https://onlinelibrary.wiley.com/terms-and-conditions) on Wiley Online Library for rules of use; OA articles are governed by the applicable Creative Commons License

Table 1
Input Parameters for the Eight AIKEF Simulations Covering a Full Synodic Period T[a]

Ωt (°)	λ_{III} (°)	$[B_{x,0}, B_{y,0}, B_{z,0}]$ (nT)	$\lvert\mathbf{B}_0\rvert$ (nT)	$\lvert\mathbf{v}_{A,0}\rvert$ (km/s)	M_A	n_0 (cm^{-3})	Position w.r.t the current sheet
0	11	[−13.3, +201.3, −396.5]	444.9	357.3	0.28	40	Below
45	56	[+41.2, +181.5, −407.0]	447.5	288.0	0.35	63	Transition into
90	101	[+82.8, +39.2, −415.2]	425.2	156.6	0.64	191	Within
135	146	[+64.7, −142.6, −420.3]	448.5	218.9	0.46	109	Transition out of
180	191	[−3.14, −221.7, −417.9]	473.1	389.2	0.26	38	Above
225	236	[−57.8, −152.2, −405.5]	436.9	255.3	0.39	76	Transition into
270	281	[−66.3, −9.66, −391.6]	397.3	143.3	0.70	199	Within
315	326	[−48.1, +122.5, −388.5]	410.1	220.7	0.45	89	Transition out of

[a]The quantity λ_{III} denotes Europa's System III longitude at the respective value of Ωt; $M_A = \frac{|\mathbf{u}_0|}{|\mathbf{v}_{A,0}|}$ is the Alfvénic Mach number, with Alfvén velocity $\mathbf{v}_{A,0} = \frac{\mathbf{B}_0}{\sqrt{n_0 m_0 \mu_0}}$.

Upstream parameters for each of the eight distances to the plasma sheet are provided in Table 1. For all simulations, we assume that the Jovian magnetospheric ions have an average mass of $m_0 = 18.5$ amu with a velocity of $\mathbf{u}_0 = [100, 0, 0]$ km/s. We allow the ambient Jovian magnetospheric field $\mathbf{B}_0$ and plasma density n_0 to vary as a function of Europa's distance to the Jovian plasma sheet (but not within a single AIKEF simulation) using the models of Connerney et al. (2020, 2022) and Roth et al. (2014), respectively. Although we choose locations that are equally spaced in System III longitude (λ_{III}), the magnetic field and plasma density are not exactly mirrored between two positions separated by 180°. This is in part explained by recent findings from the Juno mission showing that Jupiter's internal magnetic field possesses a non-negligible north/south asymmetry, likely driven by non-uniformities within the planetary dynamo (Connerney et al., 2020; Moore et al., 2018), as well as by hinging of the magnetodisc (Khurana, 1992). Similarly, the magnetospheric density is slightly asymmetric, representing uncertainties in the plasma environment near Europa, which even displays variability between two encounters located at similar System III longitudes (cf., e.g., Allegrini et al., 2024; Bagenal & Delamere, 2011; Ebert et al., 2025; Kim et al., 2020; Kurth et al., 2001; Roth et al., 2014).

For this study, we represent Europa's atmosphere as comprised of O_2, with a surface number density of $5 \cdot 10^7$ cm^{-3} and a scale height of 100 km (see also Addison et al., 2021; Arnold et al., 2019). Although recent studies have found that surface sputtering by incident magnetospheric plasma (e.g., Addison et al., 2023) or diurnal effects (e.g., Oza et al., 2019) generate asymmetries in Europa's neutral envelope, we treat the atmosphere as spherically symmetric in order to isolate the influence of the time-varying plasma interaction currents on the resulting inductive response. Besides, these values are consistent with column density observations (Hall et al., 1995, 1998) and a radially symmetric atmosphere has been used by various modeling studies of Europa's plasma interaction (e.g., Baskevitch et al., 2025; Blöcker et al., 2016; Cervantes & Saur, 2022). Additional minor species have also been observed to comprise Europa's neutral envelope (e.g., atomic oxygen or atomic and molecular hydrogen; see Carberry Mogan et al., 2024), but their low densities and masses compared to molecular oxygen means that their influence on the global magnetic field perturbations driven by the plasma interaction are negligible.

Within AIKEF, Europa's atmosphere is ionized via uniform magnetospheric electron impacts, which is the dominant ionization mechanism by at least an order of magnitude (Carberry Mogan et al., 2023; Saur et al., 1998). Such a uniform treatment of electron impact ionization has been found to well represent the magnetic perturbations observed during multiple Galileo encounters of the moon (e.g., Arnold et al., 2019; Blöcker et al., 2016; Harris et al., 2021; Jia et al., 2018; Rubin et al., 2015; Schilling et al., 2007). This process corresponds to an "effective" collision frequency within the ionosphere which functions identically to the mass loading terms in the equations of motion for the ions (Neubauer, 1998). Recent observations during the Juno flyby have identified transient field-aligned electron beams would represent an additional, highly localized ionization mechanism of the ionosphere (Allegrini et al., 2024; Cervantes et al., 2025). However, since there is no information on how this feature near Europa would evolve over a synodic period, and because such an additional ionization mechanism

21699402, 2026, 11, Downloaded from https://agupubs.onlinelibrary.wiley.com/doi/10.1029/2026JA036129 by Georgia Institute Of Technolog, Wiley Online Library on [09/11/2026]. See the Terms and Conditions (https://onlinelibrary.wiley.com/terms-and-conditions) on Wiley Online Library for rules of use; OA articles are governed by the applicable Creative Commons License

has not been required to explain magnetic field data from Europa during the Galileo era, is not included in this study.

Schilling et al. (2007) previously investigated Europa's inductive response to the time-varying plasma interaction. The MHD approach used in that study does not capture, for example, the flow shear between the fast magnetospheric and slow ionospheric pick-up ions near Europa. Within the moon's wake and along its flanks, this triggers magnetic field perturbations at the interface between these populations. In addition, instead of including Europa within the simulation, the MHD model from Schilling et al. (2007) introduced a "virtual plasma" to mimic the magnetospheric plasma interaction with the moon. Instead of a plasma-free interior through which the Jovian magnetospheric field can diffuse, that study prescribed a density within Europa that was adjusted at each time step to artificially reduce the magnetic Reynolds number and promote magnetic field diffusion through the "obstacle." With this approach Schilling et al. (2007) successfully reproduced magnetometer data observed at the altitude of the Galileo spacecraft along its flyby trajectories. However, since Europa Clipper will reach closest approaches that are 10 times lower than those achieved during the Galileo era (Cangahuala et al., 2025), characterizing the perturbations closer to the surface is necessary to obtain reliable predictions of the magnetic environment for this mission.

Instead of using an MHD model with these limitations, we apply a hybrid approach. This formalism treats ions as particles, allowing for a self-consistent representation of flow shear between the different ion species near Europa and capturing the electromagnetic perturbations at the confluence of these distinct populations. Additionally, AIKEF treats Europa as a solid body, the inside of which is free of plasma since particles are deleted as they impact the surface. Within the interior, a non-uniform resistivity profile allows each simulation to solve the diffusion equation for the magnetic field as it propagates through the moon, preventing non-physical perturbations that may arise from the field being transported too quickly or slowly through the interior (Kriegel et al., 2009). This approach has been shown to accurately represent the magnetic field perturbations observed near the surfaces of Jupiter's icy moons (e.g., Arnold et al., 2019; Jia et al., 2009; Liuzzo et al., 2016; Stahl et al., 2023) as well as near Mercury (Jia et al., 2015, 2019).

2.3. Calculating the Inductive Response of Europa's Subsurface Ocean

Our approach seeks to establish upper limits to the contribution of induction signals from Europa's subsurface ocean that are generated by time variations in the moon's plasma interaction, in addition to the inductive response to the spatially uniform Jovian magnetospheric field. Therefore, we proceed analogous to, for example, Arnold et al. (2019) or Harris et al. (2021) and treat the moon's interior as a perfect conductor of radius $r = 1R_E$. Recently, Cervantes et al. (2025) used a multi-shell model for Europa's interior with realistic conductivities for each individual layer, and concluded that the assumption of a perfect conductor with radius $r = 1R_E$ is sufficient to accurately represent the moon's response to the time-varying Jovian magnetospheric field. This result is also consistent with the findings from Vance et al. (2021). As discussed in Section 2.1, the induced field for this step is calculated under the assumption of Europa being embedded in a vacuum. In a subsequent step, we apply AIKEF to iteratively calculate the contribution of this induced field to the plasma interaction.

Our goal in this section is to determine the induced field above Europa's surface for an arbitrarily shaped, time-varying inducing field. Hence, in contrast to the work of, for example, Zimmer et al. (2000), our considerations are not restricted to a spatially uniform inducing field. In general, the magnetic field $\mathbf{B}(r,\vartheta,\phi,t)$, as a function of time t and for $r > R_E$, can be expressed in terms of a scalar potential $\psi(r,\vartheta,\phi,t)$ with $\mathbf{B} = \nabla\psi$ and

$$\psi = \left(\psi_p + \psi_s\right)\exp(i\Omega t). \tag{5}$$

Jupiter's synodic rotation frequency Ω is the dominant excitation frequency of the inducing field near Europa and the only one that we take into account (see Section 2.1). The contribution ψ_p represents the "primary," *inducing* field (subscript p) and can be decomposed into spherical harmonics according to

$$\psi_p(r,\vartheta,\phi) = R_E\sum_{l=1}^{\infty}\sum_{m=0}^{l}\left(\frac{r}{R_E}\right)^l P_l^m(\cos\vartheta)\left\{G_l^m\cos(m\phi) + H_l^m\sin(m\phi)\right\}, \tag{6}$$

where $P_l^m(\cos\vartheta)$ denotes the Schmidt quasi-normalized associated Legendre polynomials (e.g., Vance et al., 2021). The set of Gauss coefficients G_l^m and H_l^m determines the inducing field and needs to be extracted from AIKEF output to calculate the inductive response ψ_s. This "secondary," *induced* field (subscript s) can be expressed through the potential

$$\psi_s(r,\vartheta,\phi) = R_E \sum_{l=1}^{\infty}\sum_{m=0}^{l}\left(\frac{R_E}{r}\right)^{l+1} P_l^m(\cos\vartheta)\left\{g_l^m\cos(m\phi) + h_l^m\sin(m\phi)\right\}, \tag{7}$$

with two additional sets of Gauss coefficients g_l^m and h_l^m. We now need to obtain the *un*known coefficients $\left(g_l^m, h_l^m\right)$ from the known ones $\left(G_l^m, H_l^m\right)$. For a perfectly conducting sphere, this procedure is particularly straightforward; the only boundary condition that needs to be included is

$$\left[\frac{\partial}{\partial r}\left(\psi_p + \psi_s\right)\right]_{r=R_E} = 0, \tag{8}$$

indicating that the radial component of the total (inducing plus induced) magnetic field **B** disappears at Europa's surface. In other words, the inducing field cannot penetrate into the moon's interior. Evaluating Equation 8 leads to

$$\underbrace{\left\{lG_l^m - (l+1)g_l^m\right\}}_{=0}\cos(m\phi) + \underbrace{\left\{lH_l^m - (l+1)h_l^m\right\}}_{=0}\sin(m\phi) = 0. \tag{9}$$

In order for this relation to be fulfilled at any longitude ϕ, each of the two terms marked by curly brackets needs to disappear. This yields the required relations between the Gauss coefficients of the inducing and induced fields:

$$g_l^m = \frac{l}{l+1}G_l^m \qquad \text{and} \qquad h_l^m = \frac{l}{l+1}H_l^m. \tag{10}$$

To demonstrate consistency of this set of equations with previous works, we show that this formalism encompasses the expression for the induced magnetic moment that has been employed by previous authors (e.g., Liuzzo et al., 2016 or Addison et al., 2021) as a special case. These studies considered induction in a perfectly conducting sphere, driven by a time-varying, yet spatially uniform ambient magnetospheric field. Without loss of generality, we can assume this primary field to be aligned with the $\pm\mathbf{e}_y$ direction, that is, $\mathbf{B}_p = \hat{B}\,\mathbf{e}_y\exp(i\Omega t)$ and a constant amplitude $\hat{B}$. Hence, the potential of the inducing field reads

$$\psi_p = \hat{B}y = \hat{B}r\sin\vartheta\sin\phi. \tag{11}$$

Using the associated Legendre polynomial $P_1^1 = \sin\vartheta$ reveals the only non-zero Gauss coefficient of this potential to be $H_1^1 = \hat{B}$. According to Equation 10, this translates into $h_1^1 = \hat{B}/2$ as the only non-vanishing coefficient of the induction signal. Therefore, the potential of the induced field is given by

$$\psi_s = \frac{\hat{B}R_E^3}{2}\frac{\sin\vartheta\sin\phi}{r^2} = \frac{\hat{B}R_E^3}{2}\frac{y}{r^3}. \tag{12}$$

We compare this expression to the potential of a dipole field, generated by the magnetic moment $\mathbf{M} = \left(M_x, M_y, M_z\right)$:

$$\psi_s = -\frac{\mu_0}{4\pi}\frac{\mathbf{M}\cdot\mathbf{r}}{r^3}. \tag{13}$$

The inclusion of the minus sign on the right side is intentional and consistent with our sign convention in the relation between the **B** field and its potential. Equation 13 delivers the only non-zero component of the induced dipole moment,

21699402, 2026, 11, Downloaded from https://agupubs.onlinelibrary.wiley.com/doi/10.1029/2026JA036129 by Georgia Institute Of Technolog, Wiley Online Library on [09/11/2026]. See the Terms and Conditions (https://onlinelibrary.wiley.com/terms-and-conditions) on Wiley Online Library for rules of use; OA articles are governed by the applicable Creative Commons License

$$M_y = -\frac{2\pi}{\mu_0} R_E^3 \hat{B}, \tag{14}$$

as consistent with previous studies (see, e.g., Equation 1 of Liuzzo et al. (2016) or Equation 2 of Addison et al. (2021)).

Besides the above framework, a useful tool of our analysis of induction at Europa presented in Section 3 will be to express the components of the induced magnetic moment **M** in terms of the Gauss coefficients of the dipole field. For this purpose, we inspect the dipolar $\left(\propto r^{-2}\right)$ contributions to the induction signal from Equation 7:

$$\psi_{\mathrm{dip}}(r,\vartheta,\phi) = \frac{R_E^3}{r^2}\left\{g_1^0 \cos\vartheta + \left(g_1^1 \cos\phi + h_1^1 \sin\phi\right)\sin\vartheta\right\}, \tag{15}$$

where we used $P_1^0 = \cos\vartheta$. By expressing the dipole potential from Equation 13 in spherical polar coordinates,

$$\psi_{\mathrm{dip}}(r,\vartheta,\phi) = -\frac{\mu_0}{4\pi r^2}\left\{M_x \sin\vartheta\cos\phi + M_y \sin\vartheta \sin\phi + M_z \cos\vartheta\right\}, \tag{16}$$

we then obtain the relations

$$M_x = -\frac{4\pi R_E^3}{\mu_0} g_1^1, \qquad M_y = -\frac{4\pi R_E^3}{\mu_0} h_1^1, \qquad \text{and} \qquad M_z = -\frac{4\pi R_E^3}{\mu_0} g_1^0 \tag{17}$$

between the Gauss coefficients and the induced magnetic moment.

In contrast to previous studies, the oscillation in all three components of the Jovian magnetospheric background field is included when calculating the induced dipole moment that results from the time variability of $\mathbf{B}_0$. In other words, we consider the weak time variability of $B_{z,0}$ across a synodic rotation (Table 1), which also contributes to Europa's inductive response and generates an M_z component of the induced dipole moment. Although the magnitude of this component is generally small compared to M_x or M_y (since the time-variable part of $B_{z,0}$ is small), the magnetic fields associated with this component may still be comparable in magnitude to the induction signal from, for example, time-varying plasma currents or fluid convection in the ocean.

3. Results

3.1. Iteration 1: Induction From the Jovian Background Field Alone

Figure 1 displays the B_x and B_y perturbations near Europa in the $z = 0$ plane for eight AIKEF simulations. These eight scenarios represent the results after the first iteration in our process; that is, they display the steady-state plasma interaction with Europa's ionosphere and the magnetic field induced only by the time-varying, but uniform Jovian magnetospheric background field. In this step, there is no contribution to the inductive response from the time variability of plasma interaction currents $\mathbf{B}_p$ near Europa (i.e., $\mathbf{B}_{\mathrm{ind}}(\mathbf{B}_p) = \mathbf{0}$). Each panel (a–h) in Figure 1 displays a "snapshot" of the stationary structures in Europa's interaction region at select positions representing a full synodic period T, ranging from $\Omega t = 0°$ (corresponding to a System III longitude of $\lambda_{\mathrm{III}} = 11°$) to $\Omega t = 315°$ ($\lambda_{\mathrm{III}} = 326°$). Note that while the colorbars in each panel are different to highlight the perturbation signatures (and therefore should not directly be compared between runs), they are each centered at the magnetospheric background value for the respective component (see Table 1). Perturbations above or below this background value are indicated by red and blue hues in each panel, respectively.

Europa's induced dipole maximizes when the moon is at large distances to the center of the Jovian current sheet. In Figure 1, this induced dipole is therefore strongest in panels 1a and 1e, which display the magnetic field components with Europa located far below and above the current sheet, respectively. In B_x, the induced field is most visible near the moon's wakeside surface. In a (hypothetical) scenario without the plasma interaction, the B_x signatures near Europa in this plane that are associated with the induced dipole would form four "shamrock lobes" in the four quadrants of the EPhiO system centered at the moon with alternating signs (see, e.g., Figures A1 and A2). Two of these lobes would extend into the moon's upstream hemisphere while the other two would extend

21699402, 2026, 11, Downloaded from https://agupubs.onlinelibrary.wiley.com/doi/10.1029/2026JA036129 by Georgia Institute Of Technolog, Wiley Online Library on [09/11/2026]. See the Terms and Conditions (https://onlinelibrary.wiley.com/terms-and-conditions) on Wiley Online Library for rules of use; OA articles are governed by the applicable Creative Commons License

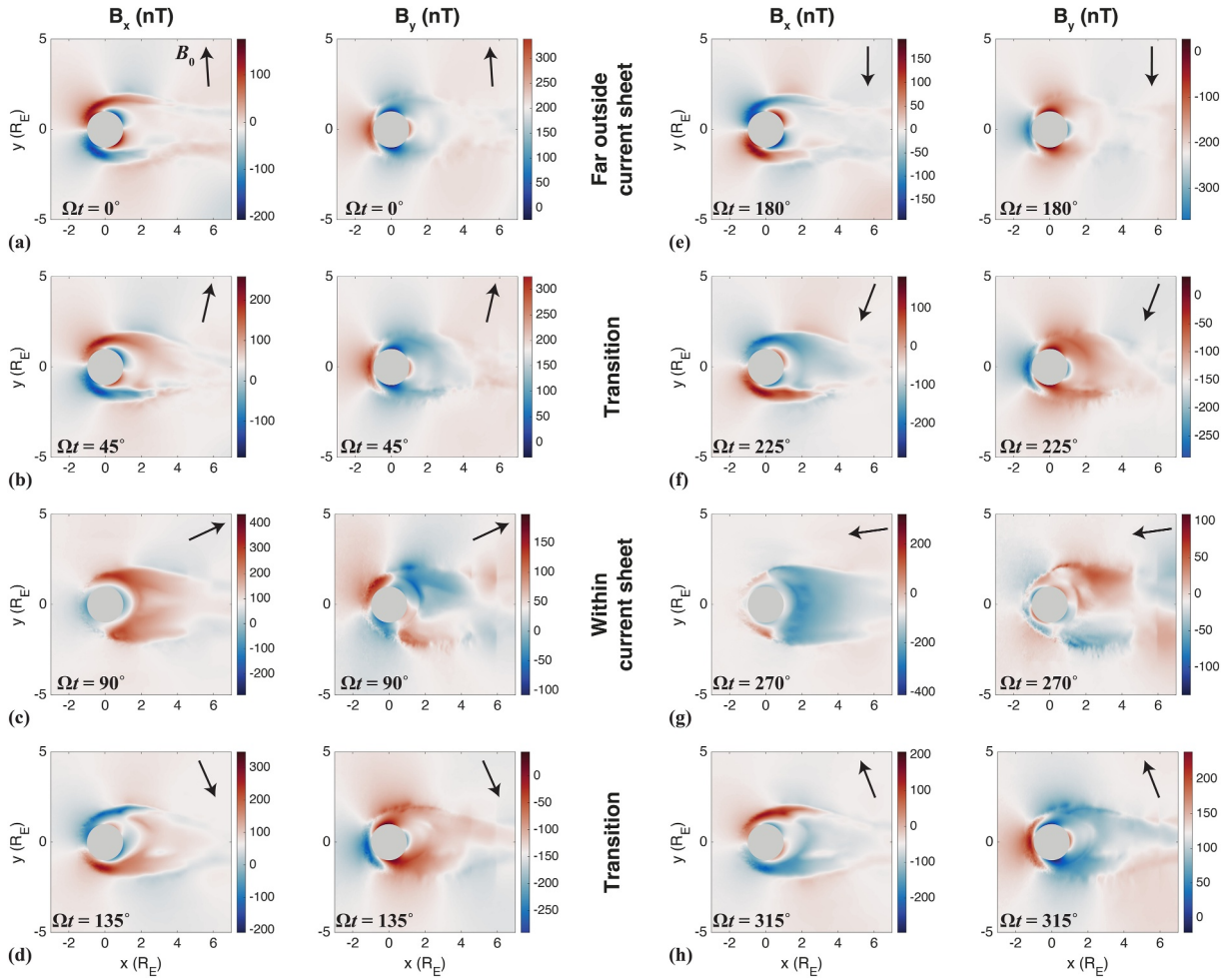


Figure 1. Magnetic field perturbations near Europa for eight snapshots in Ωt over a full synodic period T, for the first iteration ($\mathbf{B}_{\rm ind}(\mathbf{B}_p) = \mathbf{0}$). In each panel, the B_x and B_y components are shown in Europa's equatorial ($z = 0$) plane. Note the differing colorbars between the panels, which are each centered on the respective value of the Jovian magnetospheric background field ($B_{x,0}$ or $B_{y,0}$) for the specific run (see also Table 1). Arrows in each panel denote the projection of the background magnetospheric field $\mathbf{B}_0$ onto this plane, but are not to scale.

toward downstream. Panel 1a shows that upstream of Europa, magnetic field perturbations associated with the plasma interaction generate a signature in B_x that appears to merge with the two lobes from the induced field. These perturbations extend toward downstream along the moon's flanks, compressing the two lobes located downstream of the moon and confining them closer to Europa's wakeside surface (see also Liuzzo et al., 2016). In panel 1e, the sign of these lobes is reversed compared to those in panel 1a, due to the change in the orientation of $B_{0,y}$ (as denoted by the arrow projected onto each of the panels).

Europa's magnetic moment induced by the time-varying magnetospheric background field is anti-parallel to the projection of $\mathbf{B}_0$ onto the $z = 0$ plane. Hence, $|B_y|$ is reduced near the "poles" of the induced field near moon's surface in the sub- and anti-Jovian hemispheres (i.e., near $x = 0, y = \pm 1R_E$), and is enhanced near the "equator" ($y = 0, x = \pm 1R_E$). Pile-up of the Jovian magnetospheric field in Europa's upstream hemisphere generates an additional, slight enhancement in $|B_y|$ near the moon's ramside.

Progressing through a full synodic period (i.e., stepping sequentially from panels 1a–1h), the same general morphology of the plasma interaction and induced magnetic field signatures is visible near Europa, although the magnitude or orientation of the magnetic field within any specific feature varies. The most notable exception is when the moon is near the center of the Jovian magnetospheric current sheet (Figures 1c and 1g). Here, the magnitude of the inducing field associated with the time variability of the Jovian magnetospheric field minimizes but does not vanish. Hence, the magnetic perturbations visible near Europa are predominately associated with the

21699402, 2026, 11, Downloaded from https://agupubs.onlinelibrary.wiley.com/doi/10.1029/2026JA036129 by Georgia Institute Of Technolog, Wiley Online Library on [09/11/2026]. See the Terms and Conditions (https://onlinelibrary.wiley.com/terms-and-conditions) on Wiley Online Library for rules of use; OA articles are governed by the applicable Creative Commons License

21699402, 2026, 11, Downloaded from https://agupubs.onlinelibrary.wiley.com/doi/10.1029/2026JA036129 by Georgia Institute Of Technolog, Wiley Online Library on [09/11/2026]. See the Terms and Conditions (https://onlinelibrary.wiley.com/terms-and-conditions) on Wiley Online Library for rules of use; OA articles are governed by the applicable Creative Commons License

moon's plasma interaction, exceeding values of 400 nT (i.e., equal in strength to the Jovian background field). In particular, the large Alfvénic Mach number within the plasma sheet causes the Alfvén wings to be tilted more toward downstream (Neubauer, 1998) compared to a scenario with Europa located far from the center of the sheet (cf. Table 1). In addition, the non-zero $B_{x,0}$ component of the magnetospheric field causes the southern (Figure 1c) or northern (Figure 1g) Alfvén wing tube to be rotated into the geometric plasma shadow downstream of the moon. Hence, the "neutral region" between the wings where B_x returns to its background value no longer coincides with Europa's equatorial plane, generating the $B_x > 0$ or $B_x < 0$ signatures visible in these respective panels (see also Harris et al., 2021; Simon & Motschmann, 2009).

As also visible across each row of Figure 1, the B_x and B_y signatures associated with the moon's interaction and induced field are nearly symmetric with respect to distance to the sheet. When the moon's position is separated by 180° in Ωt the orientations of the magnetic field structures flip. However, since the ambient $B_{x,0}$ and $B_{y,0}$ components are not mirrored (see also Table 1), subtle quantitative differences in the plasma interaction between any two conjugate simulation pairs are visible.

After completing this first iteration of AIKEF simulations over a full synodic period T, we determine an initial estimate of the inducing magnetic field associated with the time variability of Europa's plasma interaction (see Section 2.3). Figure 2 displays the Gauss coefficients of the (a–b) dipole and (c) quadrupole terms associated with the time-varying magnetic field near the moon's orbit, distinguishing between the variabilities associated with (2a) $\mathbf{B}_0$ and (2b) the plasma perturbations. Since higher-order terms (i.e., octupole and above) are even smaller in magnitude than the dipole and quadrupole terms (see also Schilling et al., 2007), and fall-off much more rapidly, we do not consider their effects here.

Comparing Figures 2a–2c shows that the induced dipole coefficients associated with the time variability of the Jovian magnetospheric background field (dashed lines) dominate for nearly every value of Ωt by up to a factor of 20, with the peak magnitudes of the h_1^1 and g_1^1 terms reaching ∼100 nT and ∼50 nT, respectively. These terms correspond to the M_y and M_x components of Europa's induced dipole (see also Equation 17). For the g_1^0 term, the contribution from the time-varying portion of $B_{z,0}$ to the induced field introduces a small M_z component (see also Equation 17). This accounts for a maximum difference in the magnitude of the induced dipole of ∼1 nT and a change in the angle of $\mathbf{M}_{\text{ind}}$ of up to 11°, compared to the case when only considering the contributions from the time-varying $B_{x,0}$ and $B_{y,0}$ components.

Although the moon's inductive response to the (uniform) time-varying Jovian field dominates, panels 2b and 2c illustrate that the Gauss coefficients generated by the (non-uniform) time-varying plasma interaction are still responsible for an appreciable contribution to the induction signal observable at Europa's surface. The maximum value of $|\mathbf{B}_{\text{ind}}(\mathbf{B}_p)|$ associated with this set of plasma-induced coefficients exceeds a value of ∼40 nT on the surface, for the case of $\Omega t = 90°$. This is comparable to the surface magnetic field associated with differences in the subsurface ocean's composition (Vance et al., 2021) and stronger than other effects stemming from ocean asymmetries or dynamics.

For the plasma-induced dipole coefficients, two trends are visible in panel 2b. First, the g_1^1 term (associated with M_y) is nearly sinusoidal, maximizing near a value of up to +15 nT when Europa is located far from the center of the Jovian current sheet ($\Omega t = 0°$ and $\Omega t = 180°$) and minimizing near −15 nT when Europa is embedded within the sheet ($\Omega t = 90°$ and $\Omega t = 270°$). By comparison, the h_1^1 term (associated with M_x) reaches its extrema in the transitional regions near $\Omega t = 45°$ and $\Omega t = 135°$. The $g_1^0\left(M_z\right)$ dipole term visible in panel 2b reaches values of up to ±10 nT when transitioning out of the current sheet center. This coefficient therefore contributes to a maximum induced magnetic field on Europa's surface of ∼20 nT, similar to the magnitude of the contribution from the time-varying $B_{z,0}$ component of the magnetospheric background field to the moon's inductive response, but 180° out of phase with that component (cf. panel 2a).

All quadrupole coefficients induced by the time-varying plasma interaction in panel 2c remain below 5 nT in magnitude for all values of Ωt. Hence, Europa's inductive response to the time-varying plasma interaction is predominantly dipolar for all locations of Europa relative to the plasma sheet. However, for times when Europa is just outside of the center of the Jovian current sheet (e.g., near $\Omega t \approx 70°$ or $\Omega t = 225°$), these terms are similar in magnitude to the g_1^1 and h_1^1 dipole coefficients induced by the moon's time-varying plasma interaction. At these locations, their contributions result in measurable deviations from a pure dipolar signature near Europa's surface.

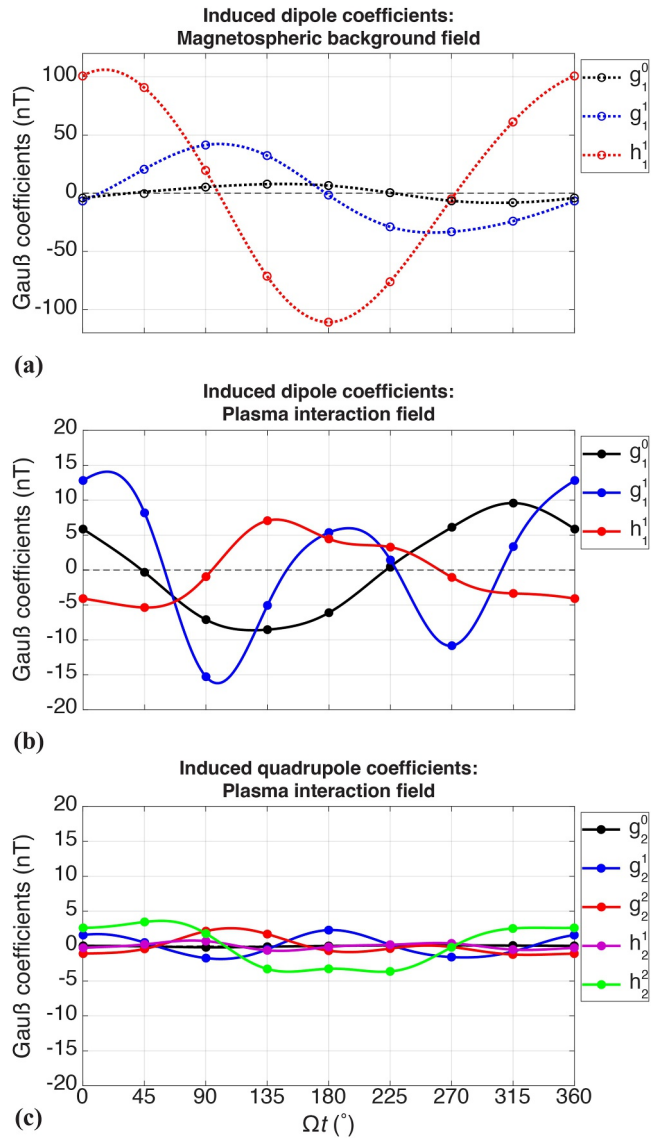


Figure 2. Gauss coefficients of the induced field associated with the time variability of the external magnetic field near Europa over a synodic period. Circles denote the eight discrete values of Ωt at which hybrid simulations were run. Dashed lines in panel (a) display the induced dipole coefficients associated with the time-varying Jovian magnetospheric background field alone, while solid lines in panels (b and c) display coefficients associated with the time-varying plasma interaction alone, for the induced (b) dipole and (c) quadrupole terms. Note the difference in the vertical axes between panels (a) and (b and c).

Our results for the Gauss coefficients display some notable differences compared to the previous findings of Schilling et al. (2007). These authors show that the g_1^1 dipole coefficient maximizes near the center of the Jovian current sheet, but remains within approximately ±3 nT at all other locations. For the quadrupole coefficients, our results illustrate that all five terms remain below values of ±5 nT throughout a full synodic period T, while Schilling et al. (2007) found variability of up to 20 nT in some of these terms. These discrepancies are likely due to the differences between the approaches in these two studies. Most importantly, Schilling et al. (2007) applied a single-fluid magnetohydrodynamic model to represent Europa's perturbed plasma environment. However, we have applied a hybrid approach for Europa's interaction that accurately resolves, for example, the relative motion between the bulk flows of ionospheric and magnetospheric plasma. Additionally, slight differences between the assumed properties of Europa's atmosphere influence the resulting plasma currents, thereby altering the inducing plasma interaction signatures. A second difference is that Schilling et al. (2007) consider the inductive response of multiple shells below the surface of Europa, while we have assumed a perfectly conducting sphere of radius $1R_E$.

21699402, 2026, 11, Downloaded from https://agupubs.onlinelibrary.wiley.com/doi/10.1029/2026JA036129 by Georgia Institute Of Technolog, Wiley Online Library on [09/11/2026]. See the Terms and Conditions (https://onlinelibrary.wiley.com/terms-and-conditions) on Wiley Online Library for rules of use; OA articles are governed by the applicable Creative Commons License

21699402, 2026, 11, Downloaded from https://agupubs.onlinelibrary.wiley.com/doi/10.1029/2026JA036129 by Georgia Institute Of Technolog, Wiley Online Library on [09/11/2026]. See the Terms and Conditions (https://onlinelibrary.wiley.com/terms-and-conditions) on Wiley Online Library for rules of use; OA articles are governed by the applicable Creative Commons License

Finally, we note that values of Ωt between these two studies is shifted by 180°: we define $\Omega t = 0°$ as the point in time when Europa is located at large distances below the Jovian current sheet, while Schilling et al. (2007) defines this time as when the moon is located far above the sheet.

Figure 3 displays the magnetic field induced by Europa's time-varying plasma interaction near the moon's space environment from the coefficients presented in Figures 2b and 2c. That is, the components of the quantity $\mathbf{B}_{\text{ind}}(\mathbf{B}_p)$ are shown for each of the eight positions within the magnetosphere. Note that because this field is calculated analytically from the coefficients in Figures 2b and 2c, it is not the total magnetic field near Europa that would be detectable by a spacecraft. Contributions from the magnetospheric background field $\mathbf{B}_0$, the field induced from the time variability of the background field $\mathbf{B}_{\text{ind}}(\mathbf{B}_0)$, and the plasma interaction $\mathbf{B}_p$ are omitted (see Equation 1). The left two columns in each row of Figure 3 display this field within Europa's equatorial ($z = 0$) plane, while the right three columns are a cross-section within the $y = 0$ plane. Since the B_z component induced by the plasma interaction is minimal within the equatorial plane, it is omitted from the figure. In each panel, red coloring denotes regions where the displayed magnetic field component is positive (i.e., aligned with the respective axis of the coordinate system) and blue coloring denotes where regions where it is negative (i.e., anti-aligned). As visible in each panel, the components of Europa's inductive response to the time-varying plasma interaction locally reach nearly ±30 nT for most positions of the moon with respect to the magnetospheric current sheet. Across all values of Ωt, the strongest signatures often occur in B_x or B_y within Europa's equatorial plane, with clear deviations from the dipolar response to the time-varying magnetospheric field.

3.2. Iteration 2: Induction From the Jovian Background Field and Europa's Plasma Interaction

Having quantified the Gauss coefficients for each value of Ωt, we re-calculate the fields associated with the interaction between the Jovian magnetospheric plasma and Europa's inductive response. However, the magnetic field induced at the moon now contains contributions from the time-varying Jovian magnetospheric field as well as from the time-varying plasma interaction (see Equation 10). Therefore, we run a new set of eight AIKEF simulations representing a full synodic period that each include this additional contribution to the moon's induced field as a time-constant boundary condition at the moon (i.e., this plasma-induced field does not evolve within a given simulation). This allows us to identify any locations where the induced field from the time-varying plasma interaction may most strongly affect the electromagnetic field perturbations near the moon.

Figure 4 displays the differences in the B_x and B_y components near Europa between the results at the end of iterations 2 and 1 within the moon's equatorial ($z = 0$) plane, and Figure 5 shows the same quantities in Europa's polar ($y = 0$) plane. For each component i, this difference is defined as $\delta B_i = B_{i,2} - B_{i,1}$, where subscripts 2 and 1 correspond to the second and first iterations of AIKEF runs, respectively. As with Figure 3, we do not include the δB_z component in the $z = 0$ plane (Figure 4) since the induced B_z nearly vanishes within Europa's equator, but it is shown in the $y = 0$ plane (Figure 5). In each figure, red hues show regions where the magnetic field component i from iteration 2 exceeds that from iteration 1, while green hues denote the opposite. Note that even though the values of $\mathbf{B}_0$ are identical for a given Ωt between these two iterations, the plasma interaction with the different representations of Europa's inductive response is non-linear. For example, the different inductive responses can "protect" the ionosphere from pick-up in different ways, affecting ionospheric outflow and the resulting magnetic signatures. Hence, these figures do not simply display the difference between $\mathbf{B}_{\text{ind}}(\mathbf{B}_p) - \mathbf{B}_{\text{ind}}(\mathbf{B}_0)$. Since these figures are generated using the differences between magnetic field output from two simulations, typical plasma interaction features (e.g., field line pileup and draping) are not immediately visible.

Across a full synodic period, the differences between the magnetic field components range between values of approximately ±40 nT. The "patchiness" visible within these figures is associated with the statistical representation of the moon's ionosphere, which inserts actual pickup ions into the simulations (compared to the continuous source term employed by previous MHD models), further exacerbated by the high spatial resolution of the grid within these regions. Taking the difference from two identical cells across the simulations therefore generates discrete patchiness in the resulting panels. However, Figures 4 and 5 illustrate that near Europa's surface, most of the large-scale differences between the iterations are caused by the presence of the plasma-induced field. The most prominent changes between the iterations visible in these two figures, especially near Europa's surface, were also present in Figure 3. For example, with Europa located at $\Omega t = 0°$ ($\lambda_{\text{III}} = 11°$), the B_x component of the plasma-induced field generates a region of reduced B_x (blue hues in Figure 3a) near the moon's sub-Jovian apex in

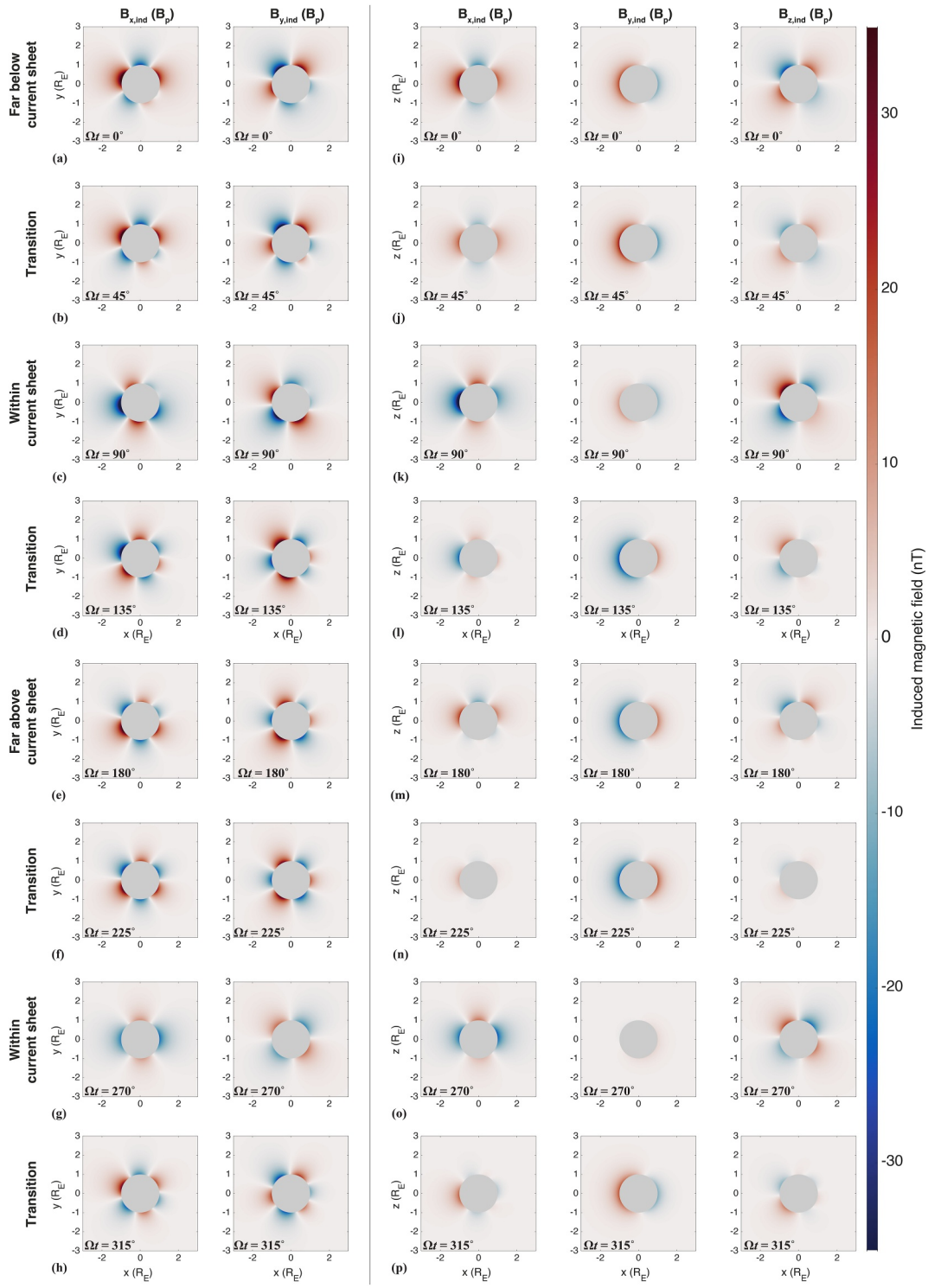


Figure 3. Europa's magnetic field induced by the time-varying plasma interaction. Panels (a–h) display the B_x and B_y components in the equatorial ($z = 0$) plane, while panels (i–p) display B_x, B_y, and B_z in the polar ($y = 0$) plane. The plasma-induced B_z component is excluded from panels (a–h) since it is weak in this plane.

21699402, 2026, 11, Downloaded from https://agupubs.onlinelibrary.wiley.com/doi/10.1029/2026JA036129 by Georgia Institute Of Technolog, Wiley Online Library on [09/11/2026]. See the Terms and Conditions (https://onlinelibrary.wiley.com/terms-and-conditions) on Wiley Online Library for rules of use; OA articles are governed by the applicable Creative Commons License

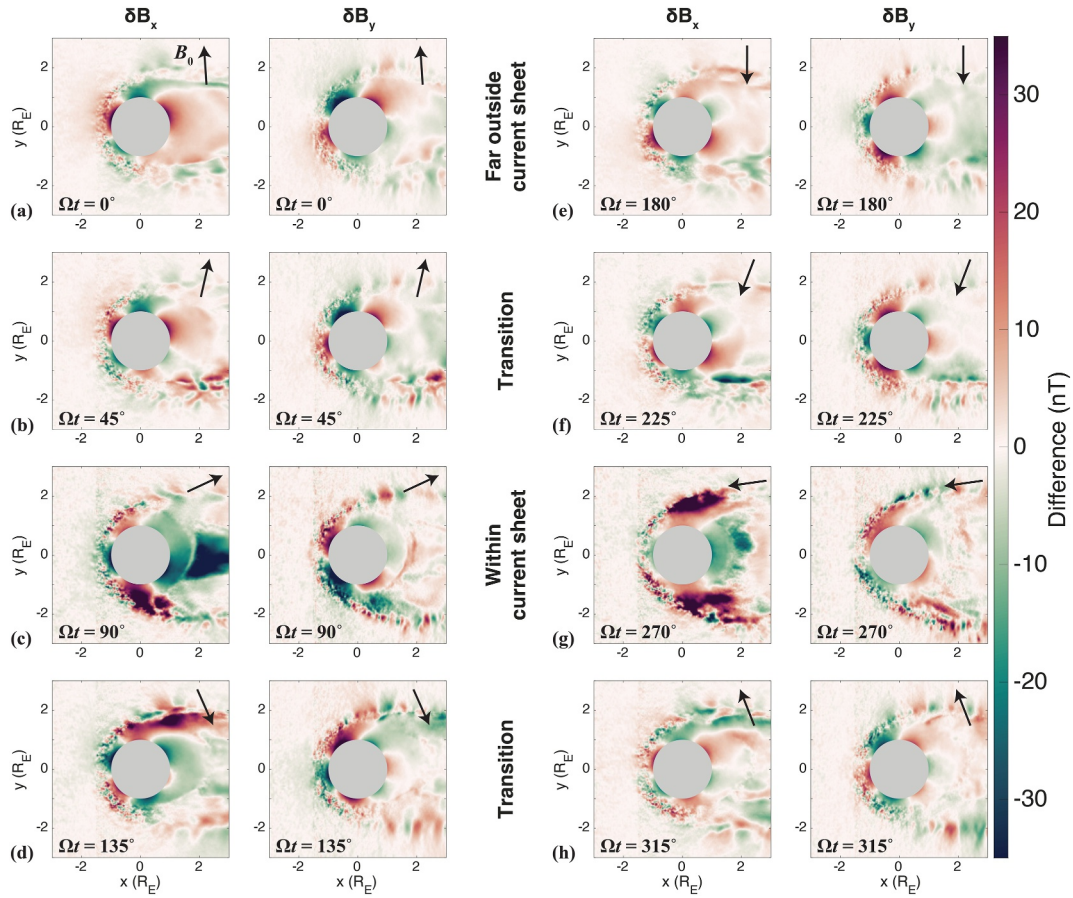


Figure 4. Difference δ in the magnetic field near Europa between AIKEF cycles (iteration 2 − 1) for select components in the equatorial ($z = 0$) plane.

the equatorial plane, surrounded on either side by regions with $B_x > 0$ extending into the upstream and downstream hemispheres (red hues in Figure 3a). On the anti-Jovian side of Europa, regions with both $B_x < 0$ (blue, upstream) and $B_x > 0$ (red, downstream) are visible. These features remain visible in Figure 4a, but are slightly deformed, compressed in Europa's upstream hemisphere and extended further downstream along the moon's flanks. Compared to iteration 1, the presence of the plasma-induced field alters the obstacle with which the magnetospheric plasma interacts. Hence, even at larger distances to Europa where the plasma-induced field itself becomes weak, the plasma interaction signatures are still affected, for example, via changing properties of the Alfvén wing tubes (see also Neubauer, 1999). Likewise in B_y, the differences between iterations 2 and 1 are consistent with the magnetospheric plasma slightly deforming the fields induced by the time-varying interaction. Similar features can be seen for all values of Ωt, especially with Europa located outside of the magnetospheric current sheet, indicating the importance of including this effect when interpreting magnetic field perturbations on the order of 10 s of nT near the moon's surface.

When the moon is located within the Jovian magnetospheric current sheet, the differences between the two scenarios are even stronger. Within the equatorial plane as the current sheet sweeps southward over the moon (panel 4c), δB_x reaches −30 nT downstream beyond $x = 3R_E$, with a spatial extent along the y direction of approximately $2R_E$. As the current sheet sweeps northward (panel 4g), the difference δB_x between the two simulations displays similar values downstream of the moon, but this region is less extended toward downstream in this plane. In addition, regions with $\delta B_x = +30$ nT have formed along Europa's flanks, which are ∼30% the magnitude of typical B_x perturbations within this region. Figure 5 shows that in the $y = 0$ plane, locations where $\delta B_x < 0$ are confined to a thin, sheet-like region when the moon is embedded within the Jovian current sheet. This feature is associated with the location between the two Alfvén wings where the B_x component reverses its sign, and illustrates the slight differences that arise between the morphology of the Alfvén wings between the two

21699402, 2026, 11, Downloaded from https://agupubs.onlinelibrary.wiley.com/doi/10.1029/2026JA036129 by Georgia Institute Of Technolog, Wiley Online Library on [09/11/2026]. See the Terms and Conditions (https://onlinelibrary.wiley.com/terms-and-conditions) on Wiley Online Library for rules of use; OA articles are governed by the applicable Creative Commons License

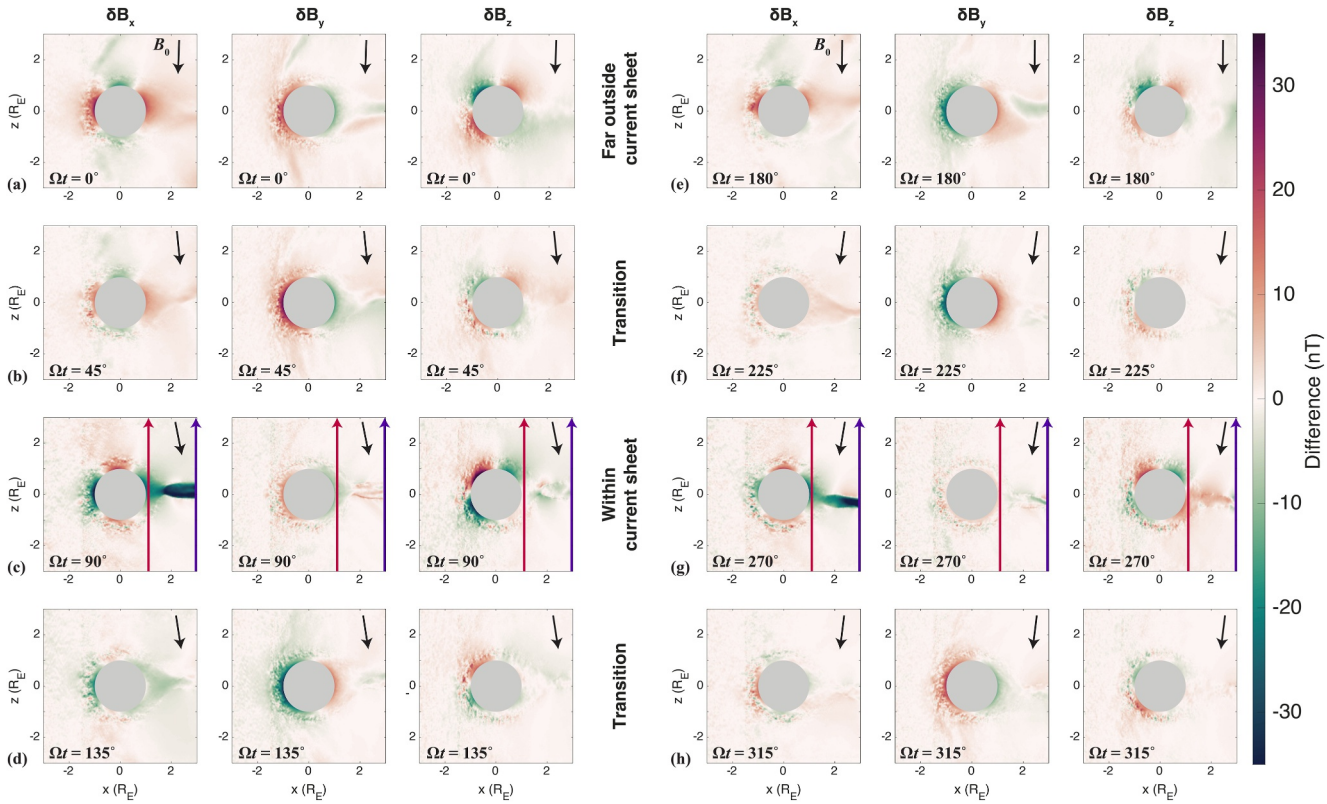


Figure 5. Same as Figure 4 but for the moon's polar ($y = 0$) plane. Vertical lines in panels (c) and (g) at $x = +1.1R_E$ and $x = +3.0R_E$ illustrate two hypothetical spacecraft trajectories along which cuts are taken in Figure 6, with arrows denoting the direction of travel.

iterations. In panel 5g, this region has been tilted slightly southward out of Europa's equatorial plane. Especially with Europa within the center of the Jovian current sheet, Figures 4 and 5 illustrate that the large values of δB_x and δB_y cannot be explained solely by differences in the inductive response. Instead, these are caused by changes in how the magnetospheric plasma interacts with the different induced fields, especially $\sim 1\ R_E$ beyond the surface where the higher-order terms (see Figures A1 and A2 for a comparison).

To further explore the contribution of the time-varying plasma interaction to Europa's induced field, Figure 6 displays magnetic field output along two hypothetical flyby trajectories located downstream of Europa. Results are shown for the two cases with Europa located at the center of the Jovian plasma sheet ($\Omega t = 90°$ and $\Omega t = 270°$), for each of the iterations (1 and 2). In each panel, pink lines denote a trajectory traveling along the z-axis taken at the position $(x, y) = (+1.1, 0)R_E$ (i.e., $\sim$150 km above the surface), while purple lines denote a trajectory traveling along the z-axis at the position $(x, y) = (+3.0, 0)R_E$. Panels 6a–f display the modeled B_x, B_y, and B_z components along these trajectories, whereas panels 6g–i display the differences (δB_x, δB_y, δB_z) along the trajectories between the two iterations at a fixed value of Ωt (see also vertical lines in Figures 5c and 5g).

Figures 6a–6f shows that for these positions of Europa within the magnetosphere, the differences between iterations 1 and 2 are mainly quantitative: runs at an identical value of Ωt display similar signatures along these sample trajectories. The most significant difference in the morphology of the perturbations between the two iterations is visible in B_y for $\Omega t = 270°$ (panel 6e) along the line located at $x = +3R_E$ (purple), near $z = -0.5R_E$. Here, the shapes of the B_y perturbations are distinct: for iteration 2 (dotted purple line), B_y gradually increases from $B_y \approx -20$ nT to a final value of $B_y \approx +3$ nT, whereas the B_y signature from iteration 1 (dashed purple line) increases above zero, then dips, before reaching the same final value. At distances of $3R_E$ downstream of Europa, these perturbations are not directly associated with differences in the moon's inductive response; instead, they are driven by the plasma interaction. Figures 6m and 6n show that this region corresponds to the location where the hypothetical flyby passes from Europa's southern Alfvén wing into the northern wing. Differences between Europa's inductive response (i.e., between iterations 1 and 2) therefore introduce changes to the

21699402, 2026, 11, Downloaded from https://agupubs.onlinelibrary.wiley.com/doi/10.1029/2026JA036129 by Georgia Institute Of Technolog, Wiley Online Library on [09/11/2026]. See the Terms and Conditions (https://onlinelibrary.wiley.com/terms-and-conditions) on Wiley Online Library for rules of use; OA articles are governed by the applicable Creative Commons License

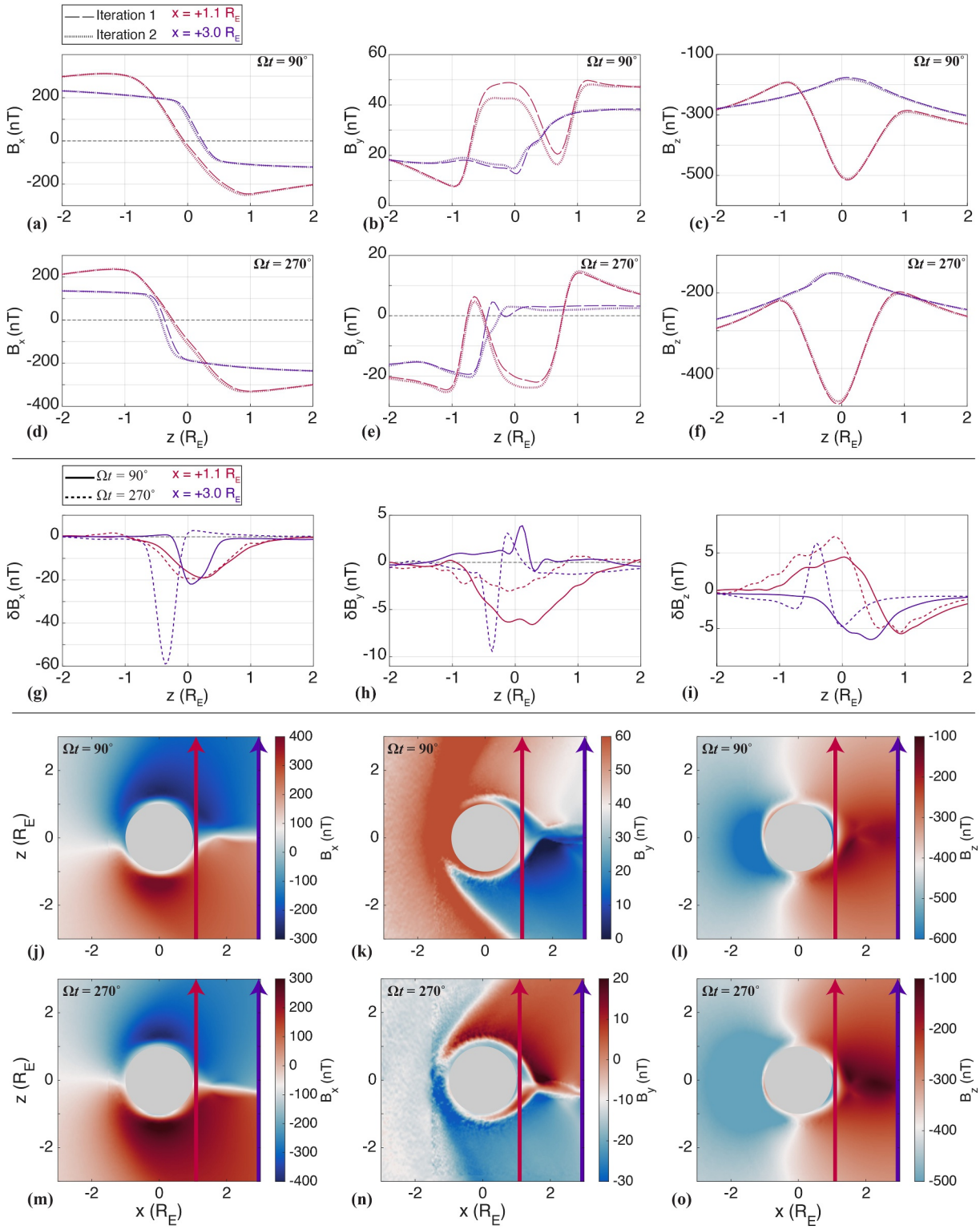


Figure 6. Magnetic field components, and differences between iterations, near Europa. Panels (a–i) display components and differences along two hypothetical flyby trajectories in the $y = 0$ plane. In panels (a–f), dashed lines indicate results for iteration 1 while dotted lines show results for iteration 2 when the moon is located near the center of the Jovian plasma sheet and the plasma interaction is strongest; that is, for (a–c) $\Omega t = 90°$ and (d–f) $\Omega t = 270°$. Panels (g–i) display the differences (iteration 2 minus iteration 1) in the components along the same trajectories. Panels (j–o) display magnetic field components as output from the hybrid simulations for (j–l) $\Omega t = 90°$ and (m–o) $\Omega t = 270°$ from iteration 2 in the $y = 0$ plane. Colored vertical lines denote the location of the same hypothetical flybys explored in panels (a–i).

21699402, 2026, 11, Downloaded from https://agupubs.onlinelibrary.wiley.com/doi/10.1029/2026JA036129 by Georgia Institute Of Technolog, Wiley Online Library on [09/11/2026]. See the Terms and Conditions (https://onlinelibrary.wiley.com/terms-and-conditions) on Wiley Online Library for rules of use; OA articles are governed by the applicable Creative Commons License

21699402, 2026, 11, Downloaded from https://agupubs.onlinelibrary.wiley.com/doi/10.1029/2026JA036129 by Georgia Institute Of Technolog, Wiley Online Library on [09/11/2026]. See the Terms and Conditions (https://onlinelibrary.wiley.com/terms-and-conditions) on Wiley Online Library for rules of use; OA articles are governed by the applicable Creative Commons License

magnetospheric plasma that manifest at large distances from the moon. The role of the non-zero $B_{x,0}$ component of the magnetospheric field between the two values of Ωt are also visible at these distances: the southern Alfvén wing ($B_x > 0$) intersects the $z = 0$ plane in panel 6j, while the northern wing ($B_x < 0$) intersects this plane in panel 6m.

Elsewhere, the differences along the sample trajectories are on the order of 10 s of nT, consistent with Figures 4 and 5. Panels 6g–6i show that the most prominent deviations occur in B_x, with the largest reaching a value of $\delta B_x = -50$ nT at distances $3R_E$ downstream of Europa's wakeside surface near $z = -0.5R_E$. However, the morphology of the signatures is similar between the two runs. As visible in Figures A2c and A2g, these are not driven by differences to Europa's inductive response alone, since the induced field at these distances nearly vanishes. Instead, the location where B_x switches sign from $B_x > 0$ to $B_x < 0$ changes between the different iterations, generating the large (negative) values of δB_x. That is, the plasma interaction with Europa's induced magnetic field in iteration 2 slightly modifies the position of certain features of the moon's interaction (e.g., the exact location where the trajectory passes from one Alfvén wing to the other; see especially panels 6g, 6j, and 6m), appearing as large differences between the two iterations.

4. Implications of Our Study

At this point, the process described in Section 2.1 may continue: one could determine Europa's inductive response from these (new) coefficients, import the induced field into AIKEF and re-run the simulations for each of the eight locations of the moon in the Jovian magnetosphere. However, after calculating the Gauss coefficients at the end of the second iteration of hybrid simulations, we found that the differences between the sets of coefficients were, on average, below 3% for the dipole and quadrupole terms alike. Hence, consistent with the results of Schilling et al. (2007), these small changes indicate that our iterative approach has converged after two steps. In addition, the spectral power of the plasma-induced Gauss coefficients is well separated with distinct peaks, indicating that discretization of the full synodic period into eight points in time is sufficient to resolve the resulting inductive response, as also indicated by Schilling et al. (2007).

To show this in a quantitative way, Figure 7 displays the ratio ϱ of the induced field at Europa's surface generated by the plasma interaction $\mathbf{B}_{\mathrm{ind}}(\mathbf{B}_p)$ after a given iteration, compared to the induced field at the surface generated by the Jovian magnetospheric field $\mathbf{B}_{\mathrm{ind}}(\mathbf{B}_0)$ alone, over a full synodic period (i.e., $\varrho = \frac{|\mathbf{B}_{\mathrm{ind}}(\mathbf{B}_p)|}{|\mathbf{B}_{\mathrm{ind}}(\mathbf{B}_0)|}$). This ratio is calculated analytically from the Gauss coefficients, but we remind the reader that the plasma-induced field does not exist "in isolation" since the inductive response to the time-varying magnetospheric background field is also present. Solid lines denote this ratio averaged over 10,000 equidistant points distributed across Europa's surface, whereas the shaded regions illustrate the range in the value of this ratio. The Gauss coefficients used to determine the inductive response calculated from iteration 1 are displayed in Figure 2. Figure 7 illustrates that the differences between the values of ϱ calculated using the results from (blue) iteration 1 and (red) iteration 2 indeed remain within a few percent of one another. That is, the induced magnetic fields that would be input into a third iteration are nearly identical to those calculated at the end of iteration 2. The most notable change occurs in the range of these ratios, which are slightly broader across all values of Ωt for iteration 2 compared to iteration 1.

Figure 7 illustrates an important point: at Europa's surface, the magnetic field induced by the time-variable plasma interaction can be comparable in magnitude to the field induced by the Jovian magnetospheric field. Especially near the center of the Jovian current sheet where the horizontal component of $|\mathbf{B}_0|$ minimizes and the perturbations associated with the plasma interaction maximize (i.e., $\Omega t = 90°$ and 270°), the contribution of plasma currents to Europa's inductive response become non-negligible. The plasma-induced field averaged across the surface exceeds a value that is ∼40% of the background-induced field, and locally exceeds 95% the value of the background-induced field within the magnetospheric current sheet. In addition, just as Europa's plasma interaction is not an exact reflection at values of Ωt that are separated by 180° (see, e.g., Figures 4 and 5) the value of ϱ is not symmetric between conjugate pairs of Ωt. For example, for the two cases of Europa within the magnetospheric current sheet, the surface-averaged ratio is similar (∼0.34–0.41), but the range in values is larger for $\Omega t = 90°$ compared to $\Omega t = 270°$. This occurs because the Jovian magnetospheric background field, plasma interaction, and hence Europa's inductive response are not exactly mirrored between these two locations. Finally, we again emphasize that, due to our assumption of a perfect conductor with radius $1R_E$, these results represent an upper limit to Europa's inductive response from the time-variable plasma interaction. Still, (Cervantes et al., 2025) have

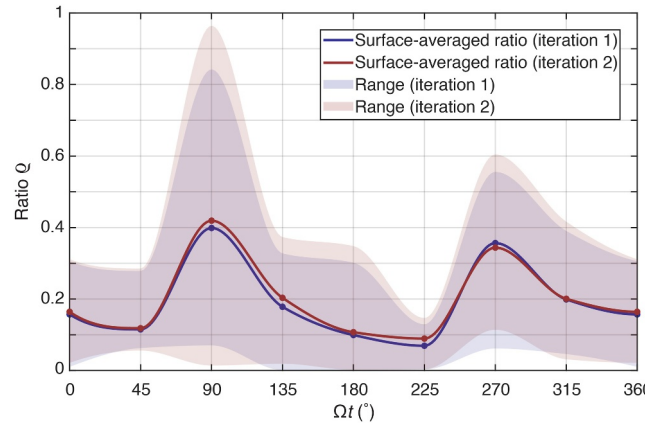


Figure 7. Ratio ϱ of the surface magnetic field magnitude induced by the plasma interaction compared to that induced by the (uniform) Jovian magnetospheric field $\mathbf{B}_0$. The Gauss coefficients used to calculate the plasma-induced response are obtained after completion of the AIKEF runs for iterations (blue) 1 (as also displayed in Figure 2) and (red) 2. Solid lines display this ratio averaged over equidistant points across Europa's surface, whereas the shaded regions display the maxima and minima that occur at any single point on the surface.

recently predicted that Europa's inductive response has an amplitude of $A = 0.96$ with a phase shift of only a few degrees, suggesting that the perfect conductor approach applied here is an adequate and justified approximation to represent the moon's response.

Since Figure 7 displays the magnetic field ratio ϱ at Europa's surface, it is not suitable to aid in interpretation of spacecraft data that is collected above the moon's surface. For example, the closest approach altitude during any Europa Clipper encounter is anticipated to be on the order of 25 km (Cangahuala et al., 2025; Pappalardo et al., 2024). Therefore, Figure 8 displays the value of this same ratio ϱ obtained at the end of iteration 2, but on a spherical shell at an altitude of 25 km above the surface. These "maps" are displayed using the West Longitude system: within Europa's equatorial plane, 0°W points toward Jupiter, 90°W is aligned with the moon's orbital leading apex, 180°W coincides with the anti-Jovian apex, and 270°W is aligned with the trailing apex (i.e., the sub-ram point of the incident magnetospheric plasma). In latitude, 90°N and 90°S represent the locations of the moon's north and south poles, respectively.

Figure 8 displays these maps for two locations of Europa within the Jovian magnetosphere, at (panel 8a) $\Omega t = 90°$ and (panel 8b) $\Omega t = 0°$. Hence, these correspond to Europa being either embedded within the Jovian current sheet ($\Omega t = 90°$) or located far below it ($\Omega t = 0°$), representing two scenarios where the plasma-induced Gauss coefficients are near their extrema. For the case of Europa embedded within current sheet, Figure 8a illustrates that the maximum value of the ratio visible in Figure 7 is not a highly localized feature. Instead, regions approaching $\varrho \approx 1.0$ cover large swaths of this altitude shell, especially concentrated between longitudes of 270°–360°W, corresponding to Europa's sub-Jovian, upstream (orbital trailing) hemisphere. That is, within this region, the contribution to Europa's inductive signal from the time-varying plasma interaction nearly equals the contribution from the time-varying Jovian magnetospheric field. Within this region, the Jovian magnetospheric background field and the magnetic moment induced by the variability of this field are nearly anti-parallel, representing a minimum in the value of $|\mathbf{B}_{\text{ind}}(\mathbf{B}_0)|$. In addition, the plasma interaction near this location causes the magnetospheric field lines to pile-up near Europa's surface, generating strong perturbations of the magnetic field that strongly varies across Ωt (see also Figure 1). Hence, Figure 8a illustrates that the interplay between these two effects (and especially their variability) causes the contribution of the plasma-induced field to maximize compared to the magnetospheric-induced field within this quadrant. However, the perturbations from field line draping when Europa is at the center of the sheet are also at their maximum, complicating the retrieval of this signature without accurate modeling of the moon's electromagnetic environment during a given flyby.

Conversely, panel 8a shows that this ratio is reduced within the upstream hemisphere at southern latitudes, locally reaching values below $\varrho \lesssim 0.3$. A similar global pattern is visible for the case with Europa located far from the sheet displayed in Figure 8b. The ratio for this scenario is comparatively reduced to below $\varrho \lesssim 0.4$ everywhere, but with the maxima and minima remaining located in similar regions across this 25 km altitude shell.

21699402, 2026, 11, Downloaded from https://agupubs.onlinelibrary.wiley.com/doi/10.1029/2026JA036129 by Georgia Institute Of Technolog, Wiley Online Library on [09/11/2026]. See the Terms and Conditions (https://onlinelibrary.wiley.com/terms-and-conditions) on Wiley Online Library for rules of use; OA articles are governed by the applicable Creative Commons License

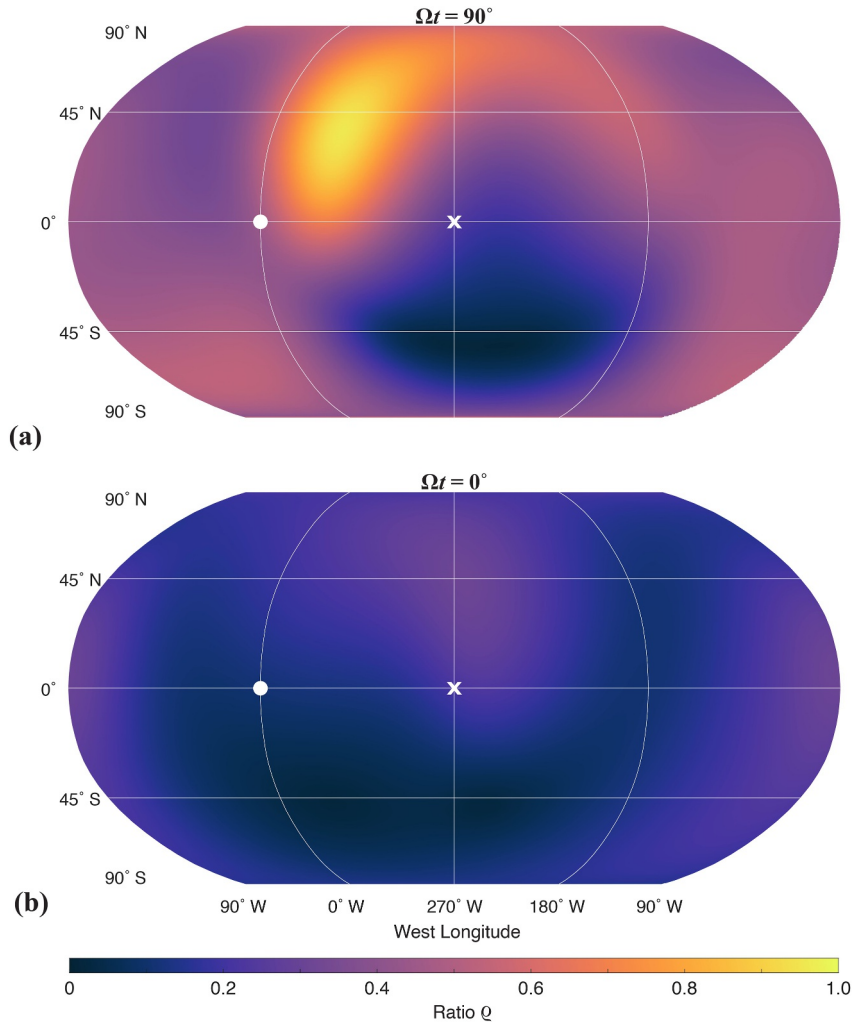


Figure 8. Ratio ϱ of the magnetic field magnitude induced by the plasma interaction compared to that induced by the (uniform) Jovian magnetospheric field plotted onto a spherical "surface" at an altitude of 25 km above Europa, in the absence of plasma interaction currents. The two panels display the cases with Europa located (a) at the center of the Jovian current sheet for $\Omega t = 90°$ and (b) far below the sheet for $\Omega t = 0°$. The white • and x in each panel denote the moon's sub-Jovian and orbital trailing hemispheres, respectively.

Overall, Figures 3–8 show that the contribution from the time-varying plasma interaction to Europa's inductive response translates to deviations on the order of 40 nT, possibly visible compared to the induction signal generated by the time variability of $\mathbf{B}_0$ even at to the expected Clipper flyby altitudes of ∼25 km. To place these effects into a more tangible context, previous studies have shown that differences in the assumed properties of the moon's interior can generate deviations up to a similar value. These properties include small "pockets" of conducting water that are isolated from a global ocean (Winkenstern & Saur, 2023), slight modifications in the composition or conductivity profile of the ocean, or even (fluid) currents associated with ocean dynamics (Vance et al., 2021; Šachl et al., 2024). Our results demonstrate that the time variability of Europa's plasma interaction generates magnetic field signatures that are at least as strong as (if not stronger than) these geophysical effects. At the closest Clipper flyby altitudes, the inductive response to plasma effects generates large spatial regions where the differences are up to 95% of the value considering induction by the time-varying magnetospheric field, alone.

In addition, the magnetospheric plasma interaction with these plasma-induced fields causes perturbations with magnitudes that are similar to those expected from different interior properties, even manifesting far beyond the surface. For example, differences in the magnetic field perturbations generated by the interaction with and without these plasma-induced fields included can reach values of 40 nT multiple R_E downstream of the moon. These

21699402, 2026, 11, Downloaded from https://agupubs.onlinelibrary.wiley.com/doi/10.1029/2026JA036129 by Georgia Institute Of Technolog, Wiley Online Library on [09/11/2026]. See the Terms and Conditions (https://onlinelibrary.wiley.com/terms-and-conditions) on Wiley Online Library for rules of use; OA articles are governed by the applicable Creative Commons License

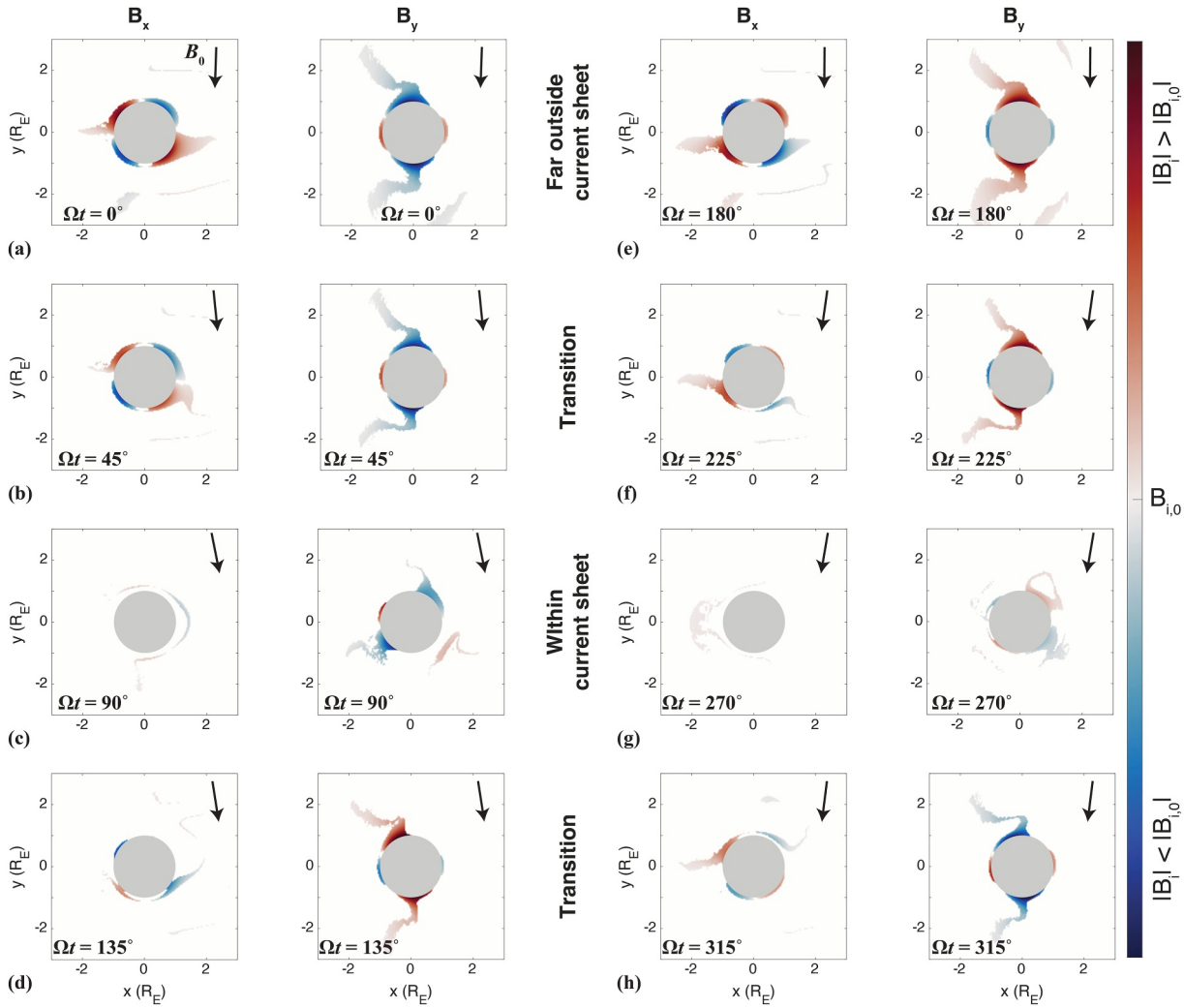


Figure 9. Locations near Europa where individual magnetic field components can be described by a superposition of the Jovian background field and the induction signal, despite the presence of plasma interaction effects. Colored regions indicate where $|B_{p,i}| < |B_{\mathrm{ind},i}|$ for component $i = x, y$, with (red) $|B_i| > |B_{i,0}|$ and (blue) $|B_i| < |B_{i,0}|$.

represent locations well beyond those regions where higher-order perturbations from, for example, differences driven by the assumed composition of an ocean could be detected. It is therefore imperative to accurately describe these effects associated with the plasma interaction on a flyby-to-flyby basis during any future Europa encounters.

In this light, we can further apply our findings to identify regions near Europa where the magnetic field can be well-described by a superposition of the Jovian background field and the moon's inductive response. This is shown in Figure 9, which highlights such locations near Europa as they change over a full synodic period and presents hybrid simulations results in the same style as Figure 1, in the moon's equatorial plane showing the results from iteration 2. Since the inductive signature in the B_z component within the equatorial plane is minimized, we exclude it from the figure. Each panel in Figure 9 uses a color scale that is identical to that of the corresponding panel in Figure 1, and the red and blue regions included in this figure correspond to locations near Europa where the following two conditions are fulfilled. First, the magnitude of magnetic field component $i = x, y$ of the induced field ($|B_{\mathrm{ind},i}|$) must exceed 5 nT. This threshold is chosen to be consistent with Winkenstern and Saur (2023), who found that individual components of Europa's induced magnetic field can be distinguished from most small-scale, random variations present in the Jovian magnetospheric field if they exceed 5 nT. Second, the magnitude of magnetic field component i generated by the plasma interaction ($|B_{p,i}|$) must be below 30% of $|B_{\mathrm{ind},i}|$; that is, the fields generated by plasma currents are small. We have chosen this threshold as a

21699402, 2026, 11, Downloaded from https://agupubs.onlinelibrary.wiley.com/doi/10.1029/2026JA036129 by Georgia Institute Of Technolog, Wiley Online Library on [09/11/2026]. See the Terms and Conditions (https://onlinelibrary.wiley.com/terms-and-conditions) on Wiley Online Library for rules of use; OA articles are governed by the applicable Creative Commons License

21699402, 2026, 11, Downloaded from https://agupubs.onlinelibrary.wiley.com/doi/10.1029/2026JA036129 by Georgia Institute Of Technolog, Wiley Online Library on [09/11/2026]. See the Terms and Conditions (https://onlinelibrary.wiley.com/terms-and-conditions) on Wiley Online Library for rules of use; OA articles are governed by the applicable Creative Commons License

conservative estimate, but found that changes to this value do not significantly affect morphology of these identified regions. Red and blue coloring in the figure then corresponds to locations where the *i*th component of the total magnetic field B_i is either (red) above or (blue) below the value of that component in the background magnetospheric plasma ($B_{i,0}$; see Table 1). All other regions in each panel (masked in white) are locations near Europa where at least one of these conditions is not met, highlighting where the magnetic field cannot reasonably be described by the sum of the background field and the induction signal.

Figure 9 illustrates that the most extended regions where the induction signal clearly exceeds the fields from plasma currents appear close to Europa's surface when located outside of the Jovian current sheet (as visible in all panels of the figure except for 9c and 9g). This is consistent with previous studies of induction at Europa and the other icy Galilean moons (e.g., Kivelson et al., 1999; Liuzzo et al., 2016; Saur et al., 2015; Zimmer et al., 2000) since far from the sheet center, Europa's inductive response to the Jovian background field maximizes and the perturbations associated with the plasma interaction minimize. Hence, there are multiple (localized) regions near the surface where the inductive response dominates the magnetic signatures from plasma currents. Even still, Figure 9 further illustrates that these regions are largely confined within ∼0.25 R_E of the moon's surface. In the B_y component, this generality is excepted in the moon's sub- and anti-Jovian hemispheres, immediately beyond the sub- and anti-Jovian antipodes. Outside of the plasma sheet, the magnetic "poles" of Europa's induced field are located near $y = \pm 1 R_E$. In these regions, the induced field is strongest and therefore less obscured by the plasma interaction. Hence, large regions with weak plasma effects (compared to the induction signal) extend to distances nearly $3R_E$ from the moon's surface. These features are sustained when Europa is located outside of the center of the Jovian current sheet, thereby representing a possibility to identify signatures of the moon's inductive response, without the need to correct for plasma effects. However, the narrow width of these regions (∼0.5 R_E) may limit the amount of time a spacecraft traveling, for example, from upstream to downstream would spend within them.

In summary, this study has quantified the role that induced fields generated by Europa's time-varying plasma interaction—and the resulting interaction itself—play on the electromagnetic field perturbations near the moon. Since our study has held all upstream, atmospheric, and interior parameters fixed between consecutive iterations at the same value of Ωt and varied only Europa's inductive response, the resulting differences can unambiguously be attributed to the presence of (and the resulting interaction with) the plasma-induced field itself. The induction signal from these time-varying plasma currents causes deviations in plasma flow and fields that may be comparable to those generated by, for example, uncertainties in the atmosphere profile or upstream conditions. Importantly, such a controlled comparison is not achievable using real spacecraft data, where ambient conditions vary and may even change during a single flyby (e.g., Kurth et al., 2001; Roth et al., 2014), so it is not possible to isolate their role in observations of the resulting perturbations near the moon. Compared to the previous study of Schilling et al. (2007), we have identified locations where the response differs from the scenario without the fields induced by Europa's time-varying plasma interaction, thereby isolating the influence of these currents on the electromagnetic perturbations outside of the moon. We have shown that the time-varying plasma interaction induces magnetic field signatures near the surface that can reach values of ∼40 nT. These perturbations are similar to those expected to be caused by, for example, non-uniformities in the shape or radial conductivity profile of the moon's subsurface ocean, when comparing to a "baseline" of a radially symmetric ocean with spatially constant conductivity. Signatures of this field are still clearly discernible even at 25 km above the moon's surface, corresponding to the locations of the low-altitude passes of the upcoming Europa Clipper mission. This inductive response and the resulting plasma interaction are therefore important to quantify on a flyby-by-flyby basis before applying magnetic field data to interpret interior properties of Europa.

Appendix A: Induced Magnetic Field in the Absence of Plasma Currents

Figures A1 and A2 display the superposition between the Jovian magnetospheric background field and the induced magnetic field, including the contribution induced by the time-variable plasma currents calculated from iteration 1, in the (A1) $z = 0$ and (A2) $y = 0$ planes. Values for each value of Ωt are shown in the (a–h) $z = 0$ and (i–p) $y = 0$ planes.

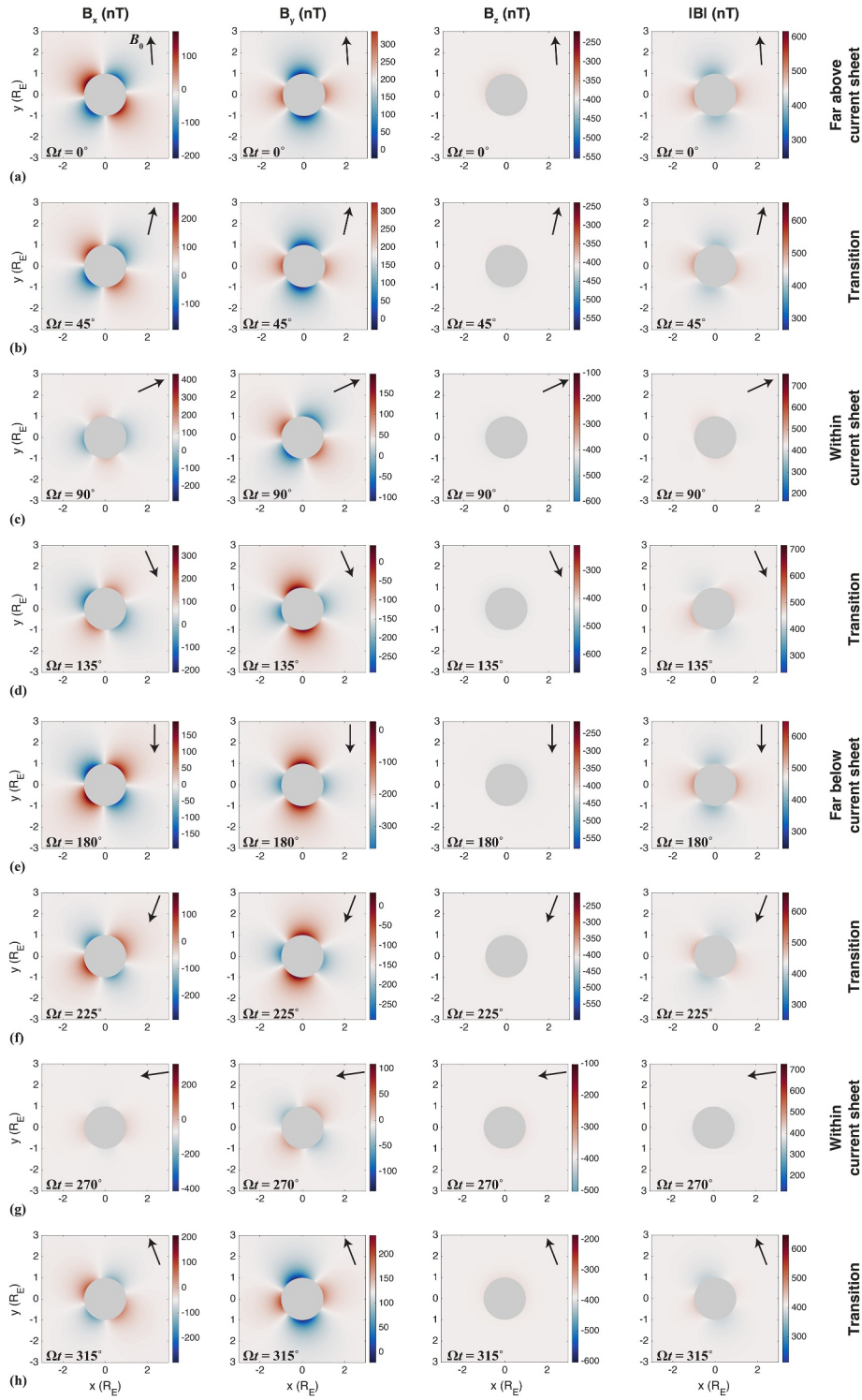


Figure A1. Superposition between the Jovian magnetospheric background field $\mathbf{B}_0$ and the induced magnetic field $\mathbf{B}_{\text{ind}}$ in the absence of plasma currents, as input into the simulations for iteration 2. Components are shown in the $z = 0$ plane.

21699402, 2026, 11, Downloaded from https://agupubs.onlinelibrary.wiley.com/doi/10.1029/2026JA036129 by Georgia Institute Of Technolog, Wiley Online Library on [09/11/2026]. See the Terms and Conditions (https://onlinelibrary.wiley.com/terms-and-conditions) on Wiley Online Library for rules of use; OA articles are governed by the applicable Creative Commons License

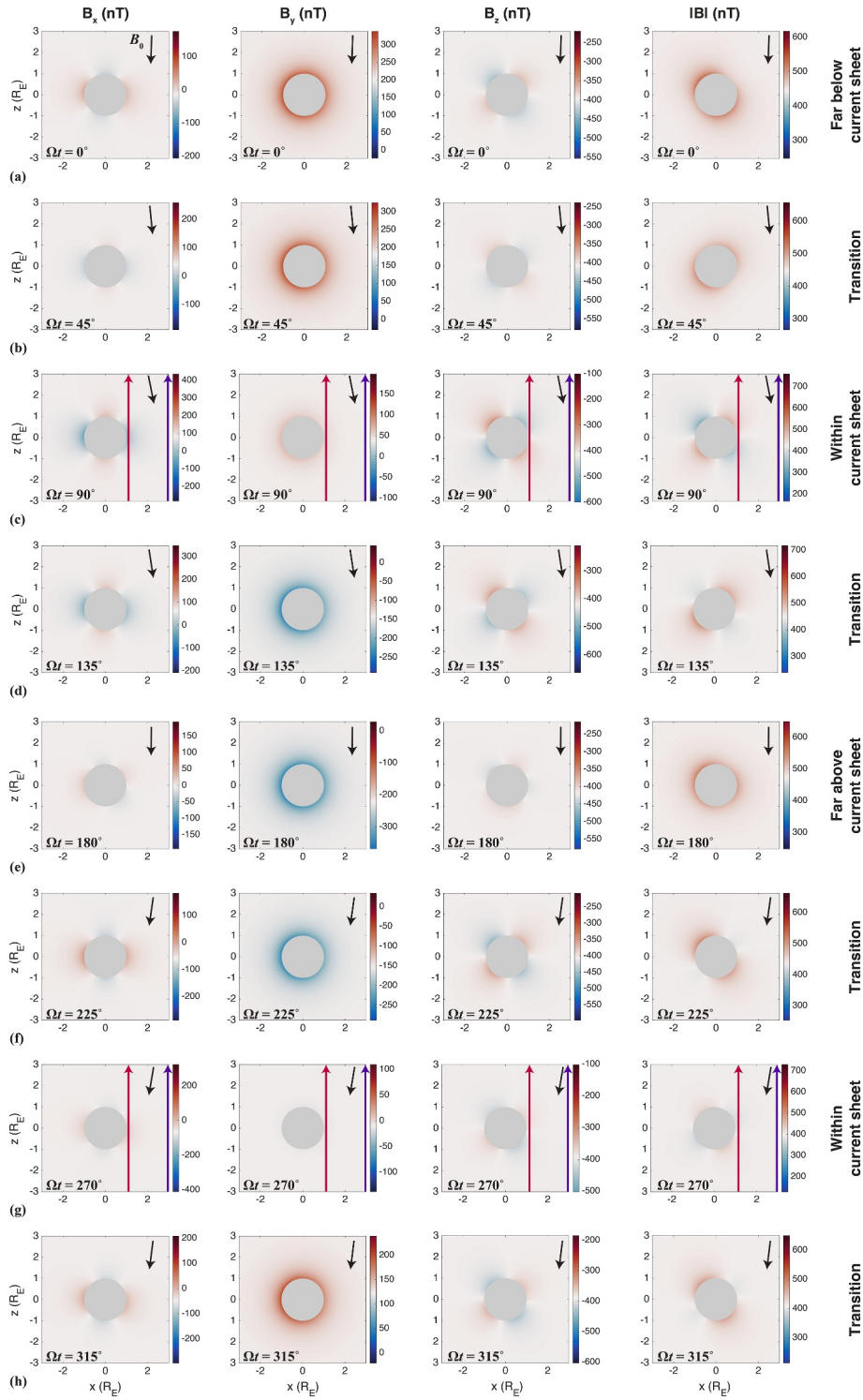


Figure A2. Same as Figure A1, but in the $y = 0$ plane. Vertical lines are as in Figure 5.

21699402, 2026, 11, Downloaded from https://agupubs.onlinelibrary.wiley.com/doi/10.1029/2026JA036129 by Georgia Institute Of Technolog, Wiley Online Library on [09/11/2026]. See the Terms and Conditions (https://onlinelibrary.wiley.com/terms-and-conditions) on Wiley Online Library for rules of use; OA articles are governed by the applicable Creative Commons License

Conflict of Interest

The authors declare no conflicts of interest relevant to this study.

Availability Statement

Results from this study can be found in Liuzzo (2026).

Acknowledgments
The authors acknowledge financial support from NASA through the Precursor Science Investigations for Europa program, Grant 80NSSC25K7618. The simulations presented in this work were completed using the NASA High-End Computing Capability provided by the Advanced Supercomputing Division at Ames Research Center.

References

Addison, P., Haynes, C. M., Stahl, A. M., Liuzzo, L., & Simon, S. (2024). Magnetic signatures of the interaction between Europa and Jupiter's magnetosphere during the Juno flyby. *Geophysical Research Letters*, *51*(2), e2023GL106810. https://doi.org/10.1029/2023GL106810

Addison, P., Liuzzo, L., Arnold, H., & Simon, S. (2021). Influence of Europa's time-varying electromagnetic environment on magnetospheric ion precipitation and surface weathering. *Journal of Geophysical Research: Space Physics*, *126*(5), e2020JA029087. https://doi.org/10.1029/2020JA029087

Addison, P., Liuzzo, L., & Simon, S. (2022). Effect of the magnetospheric plasma interaction and solar illumination on ion sputtering of Europa's surface ice. *Journal of Geophysical Research: Space Physics*, *127*(2), e2021JA030136. https://doi.org/10.1029/2021JA030136

Addison, P., Liuzzo, L., & Simon, S. (2023). Surface-plasma interactions at Europa in draped magnetospheric fields: The contribution of energetic electrons to energy deposition and sputtering. *Journal of Geophysical Research: Space Physics*, *128*(8), e2023JA031734. https://doi.org/10.1029/2023JA031734

Allegrini, F., Saur, J., Szalay, J. R., Ebert, R. W., Kurth, W. S., Cervantes, S., et al. (2024). Electron beams at Europa. *Geophysical Research Letters*, *51*(13), e2024GL108422. https://doi.org/10.1029/2024GL108422

Arnold, H., Liuzzo, L., & Simon, S. (2019). Magnetic signatures of a plume at Europa during the Galileo E26 flyby. *Geophysical Research Letters*, *46*(3), 1149–1157. https://doi.org/10.1029/2018GL081544

Arnold, H., Liuzzo, L., & Simon, S. (2020). Plasma interaction signatures of plumes at Europa. *Journal of Geophysical Research: Space Physics*, *125*(1), e2019JA027346. https://doi.org/10.1029/2019JA027346

Arnold, H., Simon, S., & Liuzzo, L. (2020). Applying ion energy spectrograms to search for plumes at Europa. *Journal of Geophysical Research: Space Physics*, *125*(9), e2020JA028376. https://doi.org/10.1029/2020JA028376

Bagenal, F., & Delamere, P. A. (2011). Flow of mass and energy in the magnetospheres of Jupiter and Saturn. *Journal of Geophysical Research: Space Physics*, *116*(A5), A05209. https://doi.org/10.1029/2010JA016294

Bagenal, F., & Dols, V. (2020). The space environment of Io and Europa. *Journal of Geophysical Research: Space Physics*, *125*(5), e27485. https://doi.org/10.1029/2019JA027485

Bagenal, F., Sidrow, E., Wilson, R. J., Cassidy, T. A., Dols, V., Crary, F. J., et al. (2015). Plasma conditions at Europa's orbit. *Icarus*, *261*, 1–13. https://doi.org/10.1016/j.icarus.2015.07.036

Baskevitch, C., Modolo, R., Cecconi, B., Leblanc, F., Wahlund, J., Aizawa, S., & Oza, A. V. (2025). Modeling Jovian plasma-Europa interactions: Innovative atmosphere and ionosphere depiction for JUICE mission insights. *Journal of Geophysical Research: Space Physics*, *130*(11), e2025JA033740. https://doi.org/10.1029/2025JA033740

Blöcker, A., Saur, J., & Roth, L. (2016). Europa's plasma interaction with an inhomogeneous atmosphere: Development of Alfven winglets within the Alfven wings. *Journal of Geophysical Research: Space Physics*, *121*(10), 9794–9828. https://doi.org/10.1002/2016JA022479

Cangahuala, L. A., Campagnola, S., Bradley, B. K., Boone, D. R., Buffington, B. B., Ludwinski, J. M., et al. (2025). Europa clipper mission design, mission plan, and navigation. *Space Science Reviews*, *221*(1), 22. https://doi.org/10.1007/s11214-025-01140-2

Carberry Mogan, S., Johnson, R., Vorburger, A., & Roth, L. (2023). Electron impact ionization in the icy Galilean satellites' atmosphere. *The European Physical Journal D*, *77*(2), 26. https://doi.org/10.1140/epjd/s10053-023-00606-8

Carberry Mogan, S., Poppe, A. R., & Liuzzo, L. (2024). The influence of non-thermal collisions in Europa's atmosphere. *Geophysical Research Letters*, *51*(20), e2024GL109534. https://doi.org/10.1029/2024GL109534

Cervantes, S., & Saur, J. (2022). Constraining Europa's subsolar atmosphere with a joint analysis of HST spectral images and galileo magnetic field data. *Journal of Geophysical Research: Space Physics*, *127*(9), e30472. https://doi.org/10.1002/jgra.v127.9

Cervantes, S., Saur, J., Duling, S., Szalay, J. R., Schlegel, S., Connerney, J. E. P., et al. (2025). MHD simulations of Europa's interaction with Jupiter's magnetosphere during the Juno flyby: Electron beams in the plasma wake. *Journal of Geophysical Research: Space Physics*, *130*(6), e2025JA033825. https://doi.org/10.1029/2025JA033825

Connerney, J. E. P., Timmins, S., Herceg, M., & Joergensen, J. L. (2020). A Jovian magnetodisc model for the Juno era. *Journal of Geophysical Research: Space Physics*, *125*(10), e2020JA028138. https://doi.org/10.1029/2020JA028138

Connerney, J. E. P., Timmins, S., Oliversen, R. J., Espley, J. R., Joergensen, J. L., Kotsiaros, S., et al. (2022). A new model of Jupiter's magnetic field at the completion of Juno's prime mission. *Journal of Geophysical Research: Planets*, *127*(2), e2021JE007055. https://doi.org/10.1029/2021JE007055

Ebert, R., Allegrini, F., Szalay, J., Pontoni, A., Saur, J., Bagenal, F., et al. (2025). Plasma and magnetic field properties in Europa's wake from Juno. *Journal of Geophysical Research: Space Physics*, *130*(5), e2024JA032520. https://doi.org/10.1029/2024ja032520

Hall, D. T., Feldman, P. D., McGrath, M. A., & Strobel, D. F. (1998). The far-ultraviolet oxygen airglow of Europa and Ganymede. *The Astrophysical Journal*, *499*(1), 475–481. https://doi.org/10.1086/305604

Hall, D. T., Strobel, D. F., Feldman, P. D., McGrath, M. A., & Weaver, H. A. (1995). Detection of an oxygen atmosphere on Jupiter's moon Europa. *Nature*, *373*(6516), 677–679. https://doi.org/10.1038/373677a0

Harris, C. D. K., Jia, X., & Slavin, J. A. (2022). Multi-fluid MHD simulations of Europa's plasma interaction: Effects of variation in Europa's atmosphere. *Journal of Geophysical Research: Space Physics*, *127*(9), e2022JA030569. https://doi.org/10.1029/2022JA030569

Harris, C. D. K., Jia, X., Slavin, J. A., Toth, G., Huang, Z., & Rubin, M. (2021). Multi-fluid MHD simulations of Europa's plasma interaction under different magnetospheric conditions. *Journal of Geophysical Research: Space Physics*, *126*(5), e2020JA028888. https://doi.org/10.1029/2020JA028888

Hartkorn, O., & Saur, J. (2017). Induction signals from Callisto's ionosphere and their implications on a possible subsurface ocean. *Journal of Geophysical Research: Space Physics*, *122*(11), 11677–11697. https://doi.org/10.1002/2017JA024269

21699402, 2026, 11, Downloaded from https://agupubs.onlinelibrary.wiley.com/doi/10.1029/2026JA036129 by Georgia Institute Of Technolog, Wiley Online Library on [09/11/2026]. See the Terms and Conditions (https://onlinelibrary.wiley.com/terms-and-conditions) on Wiley Online Library for rules of use; OA articles are governed by the applicable Creative Commons License

Haynes, C. M., Tippens, T., Addison, P., Liuzzo, L., Poppe, A. R., & Simon, S. (2023). Emission of energetic neutral atoms from the magnetosphere-atmosphere interactions at Callisto and Europa. *Journal of Geophysical Research: Space Physics*, *128*(10), e2023JA031931. https://doi.org/10.1029/2023JA031931

Haynes, C. M., Tippens, T., Simon, S., & Liuzzo, L. (2025). Constraints on the observability of energetic neutral atoms from the magnetosphere-atmosphere interactions at Callisto and Europa. *Journal of Geophysical Research: Space Physics*, *130*(1), e2024JA033391. https://doi.org/10.1029/2024JA033391

Jia, X., Kivelson, M. G., Khurana, K. K., & Kurth, W. S. (2018). Evidence of a plume on Europa from Galileo magnetic and plasma wave signatures. *Nature Astronomy*, *2*(6), 459–464. https://doi.org/10.1038/s41550-018-0450-z

Jia, X., Slavin, J. A., Gombosi, T. I., Daldorff, L. K., Toth, G., & van der Holst, B. (2015). Global MHD simulations of mercury's magnetosphere with coupled planetary interior: Induction effect of the planetary conducting core on the global interaction. *Journal of Geophysical Research: Space Physics*, *120*(6), 4763–4775. https://doi.org/10.1002/2015ja021143

Jia, X., Slavin, J. A., Poh, G., DiBraccio, G. A., Toth, G., Chen, Y., et al. (2019). Messenger observations and global simulations of highly compressed magnetosphere events at mercury. *Journal of Geophysical Research: Space Physics*, *124*(1), 229–247. https://doi.org/10.1029/2018ja026166

Jia, X., Walker, R. J., Kivelson, M. G., Khurana, K. K., & Linker, J. A. (2009). Properties of Ganymede's magnetosphere inferred from improved three-dimensional MHD simulations. *Journal of Geophysical Research*, *114*(A9). https://doi.org/10.1029/2009ja014375

Khurana, K. K. (1992). A generalized hinged-magnetodisc model of Jupiter's nightside current sheet. *Journal of Geophysical Research*, *97*(A5), 6269–6276. https://doi.org/10.1029/92JA00169

Khurana, K. K., Kivelson, M. G., Hand, K. P., & Russell, C. T. (2009). Electromagnetic induction from Europa's ocean and the deep interior. In R. T. Pappalardo, W. B. McKinnon, & K. K. Khurana (Eds.), *Europa with the assistance of René Dotson with 85 collaborating authors*. University of Arizona Press

Khurana, K. K., Kivelson, M. G., Stevenson, D. J., Schubert, G., Russell, C. T., Walker, R. J., & Polanskey, C. (1998). Induced magnetic fields as evidence for subsurface oceans in Europa and Callisto. *Nature*, *395*(6704), 777–780. https://doi.org/10.1038/27394

Kim, T. K., Ebert, R. W., Valek, P. W., Allegrini, F., McComas, D. J., Bagenal, F., et al. (2020). Survey of ion properties in Jupiter's plasma sheet: Juno JADE-I observations. *Journal of Geophysical Research: Space Physics*, *125*(4), e2019JA027696. https://doi.org/10.1029/2019JA027696

Kivelson, M. G., Jia, X., Lee, K. A., Raymond, C. A., Khurana, K. K., Perley, M. O., et al. (2023). The Europa clipper magnetometer. *Space Science Reviews*, *219*(6), 48. https://doi.org/10.1007/s11214-023-00989-5

Kivelson, M. G., Khurana, K. K., Joy, S., Russell, C. T., Southwood, D. J., Walker, R. J., & Polanskey, C. (1997). Europa's magnetic signature: Report from Galileo's pass on 19 December 1996. *Science*, *276*(5316), 1239–1241. https://doi.org/10.1126/science.276.5316.1239

Kivelson, M. G., Khurana, K. K., Russell, C. T., Volwerk, M., Walker, R. J., & Zimmer, C. (2000). Galileo magnetometer measurements: A stronger case for a subsurface ocean at Europa. *Science*, *289*(5483), 1340–1343. https://doi.org/10.1126/science.289.5483.1340

Kivelson, M. G., Khurana, K. K., Stevenson, D. J., Bennett, L., Joy, S., Russell, C. T., et al. (1999). Europa and Callisto: Induced or intrinsic fields in a periodically varying plasma environment. *Journal of Geophysical Research*, *104*(A3), 4609–4626. https://doi.org/10.1029/1998JA900095

Kivelson, M. G., Khurana, K. K., & Volwerk, M. (2009). Europa's interaction with the Jovian magnetosphere. In R. T. Pappalardo, W. B. McKinnon, & K. K. Khurana (Eds.), *Europa* (p. 545).

Kriegel, H., Simon, S., Müller, J., Motschmann, U., Saur, J., Glassmeier, K., & Dougherty, M. K. (2009). The plasma interaction of Enceladus: 3D hybrid simulations and comparison with Cassini MAG data. *Planetary and Space Science*, *57*(14–15), 2113–2122. https://doi.org/10.1016/j.pss.2009.09.025

Kurth, W., Gurnett, D., Persoon, A., Roux, A., Bolton, S., & Alexander, C. (2001). The plasma wave environment of Europa. *Planetary and Space Science*, *49*(3), 345–363. https://doi.org/10.1016/S0032-0633(00)00156-2

Liuzzo, L. (2026). Data for "Induction Signals from Europa's Subsurface Ocean: Contributions of Time Variations in the Plasma Interaction" by Liuzzo et al [Dataset]. *Zenodo*. https://doi.org/10.5281/zenodo.20736919

Liuzzo, L., Simon, S., Feyerabend, M., & Motschmann, U. (2016). Disentangling plasma interaction and induction signatures at Callisto: The Galileo C10 flyby. *Journal of Geophysical Research: Space Physics*, *121*(9), 8677–8694. https://doi.org/10.1002/2016JA023236

Moore, K. M., Yadav, R. K., Kulowski, L., Cao, H., Bloxham, J., Connerney, J. E. P., et al. (2018). A complex dynamo inferred from the hemispheric dichotomy of Jupiter's magnetic field. *Nature*, *561*(7721), 76–78. https://doi.org/10.1038/s41586-018-0468-5

Müller, J., Simon, S., Motschmann, U., Schüle, J., Glassmeier, K., & Pringle, G. J. (2011). A.I.K.E.F.: Adaptive hybrid model for space plasma simulations. *Computer Physics Communications*, *182*(4), 946–966. https://doi.org/10.1016/j.cpc.2010.12.033

Neubauer, F. M. (1980). Nonlinear standing Alfven wave current system at IO–Theory. *Journal of Geophysical Research*, *85*(A3), 1171–1178. https://doi.org/10.1029/JA085iA03p01171

Neubauer, F. M. (1998). The sub-Alfvénic interaction of the Galilean satellites with the Jovian magnetosphere. *Journal of Geophysical Research*, *103*(E9), 19843–19866. https://doi.org/10.1029/97JE03370

Neubauer, F. M. (1999). Alfvén wings and electromagnetic induction in the interiors: Europa and Callisto. *Journal of Geophysical Research: Space Physics*, *104*(A12), 28671–28684. https://doi.org/10.1029/1999JA900217

Oza, A. V., Leblanc, F., Johnson, R. E., Schmidt, C., Leclercq, L., Cassidy, T. A., & Chaufray, J.-Y. (2019). Dusk over dawn O_2 asymmetry in Europa's near-surface atmosphere. *Planetary and Space Science*, *167*, 23–32. https://doi.org/10.1016/j.pss.2019.01.006

Pappalardo, R. T., Buratti, B. J., Korth, H., Senske, D. A., Blaney, D. L., Blankenship, D. D., et al. (2024). Science overview of the Europa clipper mission. *Space Science Reviews*, *220*(4), 40. https://doi.org/10.1007/s11214-024-01070-5

Petricca, F., Cochrane, C. J., Cascioli, G., Mazarico, E., Chang, S. D., Vance, S. D., et al. (2026). Characterization of Europa's interior through synthesis of Europa clipper data. *The Planetary Science Journal*, *7*(4), 86. https://doi.org/10.3847/PSJ/ae5225

Roth, L., Retherford, K. D., Saur, J., Strobel, D. F., Feldman, P. D., McGrath, M. A., & Nimmo, F. (2014). Orbital apocenter is not a sufficient condition for HST/STIS detection of Europa's water vapor aurora. *Proceedings of the National Academy of Sciences*, *111*(48), E5123–E5132. https://doi.org/10.1073/pnas.1416671111

Rubin, M., Jia, X., Altwegg, K., Combi, M. R., Daldorff, L. K. S., Gombosi, T. I., et al. (2015). Self-consistent multifluid MHD simulations of Europa's exospheric interaction with Jupiter's magnetosphere. *Journal of Geophysical Research: Space Physics*, *120*(5), 3503–3524. https://doi.org/10.1002/2015JA021149

Šachl, L., Kvorka, J., Čadek, O., & Velímský, J. (2024). Magnetic field induced by convective flow in Europa's subsurface ocean. *Icarus*, *429*, 116375. https://doi.org/10.1016/j.icarus.2024.116375

Saur, J., Duling, S., Roth, L., Jia, X., Strobel, D. F., Feldman, P. D., et al. (2015). The search for a subsurface ocean in Ganymede with hubble space telescope observations of its auroral ovals. *Journal of Geophysical Research: Space Physics*, *120*(3), 1715–1737. https://doi.org/10.1002/2014JA020778

21699402, 2026, 11, Downloaded from https://agupubs.onlinelibrary.wiley.com/doi/10.1029/2026JA036129 by Georgia Institute Of Technolog, Wiley Online Library on [09/11/2026]. See the Terms and Conditions (https://onlinelibrary.wiley.com/terms-and-conditions) on Wiley Online Library for rules of use; OA articles are governed by the applicable Creative Commons License

Saur, J., Neubauer, F. M., & Glassmeier, K.-H. (2010). Induced magnetic fields in solar system bodies. *Space Science Reviews*, *152*(1–4), 391–421. https://doi.org/10.1007/s11214-009-9581-y

Saur, J., Strobel, D. F., & Neubauer, F. M. (1998). Interaction of the Jovian magnetosphere with Europa: Constraints on the neutral atmosphere. *Journal of Geophysical Research*, *103*(E9), 19947–19962. https://doi.org/10.1029/97JE03556

Schilling, N., Neubauer, F. M., & Saur, J. (2007). Time-varying interaction of Europa with the Jovian magnetosphere: Constraints on the conductivity of Europa's subsurface ocean. *Icarus*, *192*(1), 41–55. https://doi.org/10.1016/j.icarus.2007.06.024

Schilling, N., Neubauer, F. M., & Saur, J. (2008). Influence of the internally induced magnetic field on the plasma interaction of Europa. *Journal of Geophysical Research: Space Physics*, *113*(A3), A03203. https://doi.org/10.1029/2007JA012842

Seufert, M., Saur, J., & Neubauer, F. M. (2011). Multi-frequency electromagnetic sounding of the Galilean moons. *Icarus*, *214*(2), 477–494. https://doi.org/10.1016/j.icarus.2011.03.017

Simon, S., & Motschmann, U. (2009). Titan's induced magnetosphere under non-ideal upstream conditions: 3D multi-species hybrid simulations. *Planetary and Space Science*, *57*(14–15), 2001–2015. https://doi.org/10.1016/j.pss.2009.08.010

Stahl, A., Addison, P., Simon, S., & Liuzzo, L. (2023). A model of Ganymede's magnetic and plasma environment during the Juno PJ34 flyby. *Journal of Geophysical Research: Space Physics*, *128*(12), e2023JA032113. https://doi.org/10.1029/2023JA032113

Styczinski, M. J., & Harnett, E. M. (2021). Induced magnetic moments from a nearly spherical ocean. *Icarus*, *354*, 114020. https://doi.org/10.1016/j.icarus.2020.114020

Styczinski, M. J., Vance, S. D., Harnett, E. M., & Cochrane, C. J. (2022). A perturbation method for evaluating the magnetic field induced from an arbitrary, asymmetric ocean world analytically. *Icarus*, *376*, 114840. https://doi.org/10.1016/j.icarus.2021.114840

Vance, S., Styczinski, M. J., Bills, B. G., Cochrane, C. J., Soderlund, K. M., Gómez-Pérez, N., & Paty, C. (2021). Magnetic induction responses of Jupiter's ocean moons including effects from adiabatic convection. *Journal of Geophysical Research: Planets*, *126*(2), e06418. https://doi.org/10.1029/2020JE006418

Volwerk, M., Khurana, K., & Kivelson, M. (2007). Europa's Alfvén wing: Shrinkage and displacement influenced by an induced magnetic field. *Annales Geophysicae*, *25*(4), 905–914. https://doi.org/10.5194/angeo-25-905-2007

Winkenstern, J., & Saur, J. (2023). Detectability of local water reservoirs in Europa's surface layer under consideration of coupled induction. *Journal of Geophysical Research: Planets*, *128*(10), e2023JE007992. https://doi.org/10.1029/2023JE007992

Zimmer, C., Khurana, K. K., & Kivelson, M. G. (2000). Subsurface oceans on Europa and Callisto: Constraints from Galileo magnetometer observations. *Icarus*, *147*(2), 329–347. https://doi.org/10.1006/icar.2000.6456

21699402, 2026, 11, Downloaded from https://agupubs.onlinelibrary.wiley.com/doi/10.1029/2026JA036129 by Georgia Institute Of Technolog, Wiley Online Library on [09/11/2026]. See the Terms and Conditions (https://onlinelibrary.wiley.com/terms-and-conditions) on Wiley Online Library for rules of use; OA articles are governed by the applicable Creative Commons License